



HAL
open science

Heat transfer properties of metal, metal oxides, and carbon water-based nanofluids in the ethanol condensation process

Alireza Banisharif, Patrice Estellé, Alimorad Rashidi, Stephan van Vaerenbergh, Masoud Aghajani

► **To cite this version:**

Alireza Banisharif, Patrice Estellé, Alimorad Rashidi, Stephan van Vaerenbergh, Masoud Aghajani. Heat transfer properties of metal, metal oxides, and carbon water-based nanofluids in the ethanol condensation process. *Colloids and Surfaces A: Physicochemical and Engineering Aspects*, 2021, 622, pp.126720. 10.1016/j.colsurfa.2021.126720 . hal-03225988

HAL Id: hal-03225988

<https://univ-rennes.hal.science/hal-03225988>

Submitted on 13 May 2021

HAL is a multi-disciplinary open access archive for the deposit and dissemination of scientific research documents, whether they are published or not. The documents may come from teaching and research institutions in France or abroad, or from public or private research centers.

L'archive ouverte pluridisciplinaire **HAL**, est destinée au dépôt et à la diffusion de documents scientifiques de niveau recherche, publiés ou non, émanant des établissements d'enseignement et de recherche français ou étrangers, des laboratoires publics ou privés.

1 **Heat transfer properties of metal, metal oxides, and carbon water-based nanofluids in**
2 **the ethanol condensation process**

3 **Alireza Banisharif**^{1,2}, **Patrice Estellé**^{3,*}, **Alimorad Rashidi**⁴,

4 **Stephan Van Vaerenbergh**², **Masoud Aghajani**^{1,*}

5 ¹ Gas Engineering Department, Petroleum University of Technology, Ahwaz, Iran

6 ² Chimie-Physique (MRC), Université Libre de Bruxelles, 1050, Brussels, Belgium

7 ³ Univ Rennes, LGCGM, 35000 Rennes, France

8 ⁴ Nanotechnology Research Centre, Research Institute of Petroleum Industry (RIPI), Tehran,
9 Iran

10
11 *Corresponding authors: patrice.estelle@univ-rennes1.fr; m.aghajani@put.ac.ir

12 **Abstract**

13 This work investigates the convective heat transfer enhancement of water-based nanofluids in
14 pipe heat exchanger used for the ethanol condensation process. The nanofluids were
15 produced with different nature of nanoparticles, Cu, Fe₃O₄, MWCNT, and graphene, in the
16 volume concentration 0.01-0.1%, using different surfactants. These nanoparticles are
17 characterized by X-ray powder diffraction (XRD), Scanning electron microscopy (SEM),
18 specific surface area (BET), and Dynamic light scattering (DLS). Density, thermal
19 conductivity, and viscosity of base fluids and nanofluids were experimentally determined at a
20 relevant temperature of 20°C. Convective heat transfer enhancement under laminar regime
21 was evaluated from a well-designed experimental setup. As the main results, the thermal
22 conductivity of nanofluids increases up to 3-5% and the viscosity can increase or decrease
23 with nanoparticle concentration, showing a lubricating effect of nanoparticles coupled with
24 respective surfactant. It was shown that the heat transfer properties, heat transfer coefficient,
25 and Nusselt number, are increased with nanofluids compared to water and base-fluids, up to
26 20%, in the range of Pe 2000-10000. Experimental heat transfer properties are shown to be
27 greater than theoretical ones. Finally, copper nanofluid at low concentration appear to be the
28 best candidate for the application and pipe flow geometry considered.

29 **Keywords:** Nanofluids; Heat transfer coefficient; Laminar flow; MWCNT; Graphene; Cu;
30 Fe₃O₄

31 **Nomenclature**

32	AAD	Absolute average deviation
33	BET	Brunauer, Emmett, and Teller method
34	CH	Chitosan
35	CNT	Carbon Nanotubes
36	C _p	Heat Capacity [kJ.kg ⁻¹ .K ⁻¹]
37	D	Diameter (m or mm)
38	DLS	Dynamic Light Scattering
39	EG	ethylene glycol
40	f	friction factor
41	h	heat transfer coefficient [W m ⁻² K ⁻¹]
42	HTC	Heat Transfer Coefficient [W m ⁻² K ⁻¹]
43	L	length (m)
44	MWCNT	Multi-Walled Carbon Nanotubes
45	NFs	Nanofluids
46	NPG	Nano Porous Graphene
47	OA	oleic acid
48	PSD	Particle size distribution
49	PVP	Polyvinylpyrrolidone
50	SEM	Scanning Electron Microscope
51	SDS	sodium dodecyl sulfonate
52	T	temperature [K]
53	vol	volumetric
54	V _p	Volume of pore
55	W	water
56	WEG	water-ethylene glycol mixture
57	wt	weight
58	XRD	X-ray diffraction
59	ASHRAE	American Society of Heating, Refrigerating and Air-Conditioning Engineers handbook
60	Greek symbols	
61	α	thermal diffusivity [m ² s ⁻¹]
62	β	nanolayer thickness factor

63	$\dot{\gamma}$	shear rate [s^{-1}]
64	κ	thermal conductivity [$W\ m^{-1}\ K^{-1}$]
65	μ	dynamic viscosity [$Pa\cdot s$ or $mPa\cdot s$]
66	ρ	density [kg/m^3]
67	τ	shear rate [Pa]
68	f	volume fraction of nanoparticle

69 **Subscripts**

70	0	reference
71	b	bulk fluid
72	bf	base fluid
73	exp	experimental
74	in	inner
75	h	hydrodynamic
76	LM	Average logarithmic
77	nf	nanofluid
78	np	nanoparticle
79	out	outer
80	th	theoretical
81	wnf	at average temperature of wall

82

83

84 **1. Introduction**

85 The process of evaporation and condensation involves the transfer of heat to and from the
86 product stream, and then the change of the alcohol phase from the liquid to the vapor and vice
87 versa. This phase change requires a lot of added/removal heat at a constant temperature [1].
88 Heat exchangers can perform such a process efficiently. Recently, nanoscience and
89 nanotechnology have provided a new solution by introducing nanofluids (NFs) that can
90 ameliorate the heat transfer of thermal systems [2]. Experimental studies have shown that the
91 dispersion of solid metallic (Cu, Ag, Fe, Ni, ...), metallic-oxides (Al_2O_3 , CuO, SiC, SiO_2 ,
92 TiO_2 , Fe_2O_3 , Fe_3O_4 , ...) or carbon-based (CNT, MWCNT, graphene, graphene oxide, ...)
93 nanoparticles into the conventional base fluids can significantly enhance heat transfer

94 properties [3-6]. Most previous studies focused on the thermal and hydrodynamic properties
95 of nanofluids, and experimental studies about convective heat transfer properties and
96 coefficient evaluation are continuously growing. Main studies about the heat transfer
97 coefficients (HTC) evaluation with nanofluids in different flow regimes, laminar and
98 turbulent respectively, are summarized in [7]. The laminar flow regime is much more useful
99 to understand physical phenomena than turbulent or transitional ones, because the fluid flows
100 very regularly in the laminar flow, with a simple, smooth flow, and every particle keeps
101 moving along the streamline [7]. In the heat transfer mechanism of nanofluids, thermal
102 conductivity and dynamic viscosity of the fluids involved play important roles [8] and must
103 be rightly determined. Some relevant studies in the topic of the present work are introduced
104 hereafter.

105 Wen and Ding [9] studied the convective heat transfer of Al_2O_3 water-based nanofluids,
106 flowing through a copper tube under laminar conditions. They evidenced that heat transfer
107 rising increases with Reynolds number, particle content and mainly produces in the tube
108 entry. Heris et al. [10] investigated the convective heat transfer of CuO and Al_2O_3 water-
109 based nanofluids in a pipe in the laminar regime and fixed wall temperature. Heat transfer
110 coefficient raised with nanoparticle content and Peclet number, and be higher with Al_2O_3
111 water nanofluids. He et al. [11] studied the forced convective heat transfer of TiO_2 water-
112 based nanofluids in a vertical pipe. Heat transfer is significantly improved and shown to be
113 sensitive to nanoparticle content and flow regime. Heris et al. [12] studied heat transfer of
114 Al_2O_3 water-based nanofluid under forced convection and laminar regime in a pipe.
115 Experimentally and analytically, the results showed the convection of nanofluids is linked to
116 thermal conductivity improvement. Heat transfer enhancement reached 16% for 0.2 wt%
117 Al_2O_3 nanofluids. Garg et al. [13] examined viscosity, thermal conductivity, and laminar
118 convective heat transfer of MWCNT water-based nanofluids. It was indicated that heat
119 transfer enhancement increased by 32% and was higher than thermal conductivity
120 enhancement reaching 20%. Askari et al. [14] studied the thermal efficiency of a mechanical
121 wet cooling tower with counterflow and showed that carbon-based nanofluids are more
122 efficient than pure water. Graphene- Fe_3O_4 hybrid nanofluids with kerosene were investigated
123 in [15]. Thermal and rheological properties were studied as well as convective heat transfer
124 under constant heat flux. As the main outcome, the convective heat transfer coefficient
125 reached 66% at 0.3 wt.% and $\text{Re} \sim 4500$. Estellé et al. [16] reported thermophysical properties
126 and heat transfer efficiency of CNT water- and WEG-based nanofluids at 45°C under a

127 laminar regime. The maximum heat transfer enhancement for WEG-based nanofluids is
128 around 18.5% at 0.05 wt%, while for water-based nanofluids it is around 11.8% with the
129 same concentration. Colla et al. [17] studied the convective heat transfer of water-based TiO₂
130 nanofluids along uniformly heated pipe under laminar forced and mixed flow conditions. The
131 development of the Nusselt number along the pipe and the heat transfer with nanofluids were
132 found to be significantly different from the case of pure water. Barzegarian et al. [18]
133 investigated the thermal performance of Al₂O₃ water-based nanofluid through shell and tube
134 heat exchanger with segmental baffles. The results show a significant improvement of
135 Nusselt number as well as the total heat transfer coefficient by increasing the number of
136 Reynolds. The amount of Nusselt number of nanofluids at 0.03, 0.14, and 0.3 vol% compared
137 to base fluid is raised, by 9.7, 20.9, and 29.8%, respectively. Sadeghinezhad et al. [19]
138 reviewed the experimental results regarding graphene nanofluids' thermo-physical properties
139 and heat transfer efficiency, evidencing the relevance of these nanofluids' family as heat
140 transfer enhancers. Guzei et al. [20] investigated the laminar forced convection of Al₂O₃,
141 TiO₂, ZrO₂, and diamond nanofluids at different concentrations from 0.25 to 6 vol%. It has
142 been shown that the local and average heat transfer coefficients in the Reynold number range
143 from 10 to 1500 increase with nanoparticles content. They also illustrated that the heat
144 transfer coefficient of nanofluids in the laminar regime is dependent on the thermal-physical
145 properties of nanofluids. The effect of graphene nanofluid on a CO₂ heat pump device in a
146 heat interchanger has been studied by Wang et al. [21]. Exergy transfer in the heat exchanger
147 for graphene nanofluids at 0.01~0.1 wt.% was higher than those with 0.5~1 wt.%. Recent
148 numerical simulations of nanofluid heat transfer in laminar flow [22, 23] have demonstrated
149 that the Nusselt number, drag coefficient, pressure drop, and heat transfer coefficient increase
150 with increasing nanoparticle concentration at a specified Reynolds number. Gholami et al.
151 [24] as well as Gravndyan et al. [25] reported that the geometry of the heat transfer
152 configuration can have a significant effect on eat transfer increase with MWCNT oil and
153 TiO₂ water-based nanofluids. They investigated in particular how rib shapes affect the heat
154 transfer of nanofluid flow in a rectangular microchannel.

155 The previously cited works evidenced that heat transfer enhancement with nanofluids
156 depends on nanoparticle nature, content, and dispersion state, range of Re number,
157 temperature, thermophysical properties of nanofluids, heat exchanger configuration, ...
158 Among these parameters, low content of nanoparticles in the nanofluids is required in terms
159 of cost and operation, such as preventing blocking, instability, pump power reduction, and

160 other negative factors [26]. Because of its proneness to coagulation, nanofluids can lose their
161 ability for heat transfer. In addition, the key problem when using nanofluids is also dispersion
162 state that can change the thermo-physical properties of nanofluids and their suitability in
163 various applications. This can be improved by considering different stabilization techniques
164 such as the use of surfactants or surface functionalization of the nanoparticles before
165 dispersing them in the base fluid or other methods [27]. Consequently, a challenge is the
166 determination of surfactants' role, which is not always considered.

167 Finally, our aim is to investigate the thermal efficiency of different water-based nanofluids in
168 a heat exchanger used for the ethanol condensation process. With this goal, several
169 nanoparticles that differ in nature were considered, copper (Cu) as metallic nanoparticles,
170 Fe_3O_4 as metal oxides, and MWCNT and NPG as carbon nanoparticles respectively. This was
171 done to clearly compare the impact of nanoparticle nature on heat transfer efficiency. These
172 nanoparticles were fully characterized by XRD, SEM, BET surface area and DLS analysis.
173 These nanoparticles are used to prepare water-based nanofluids with low content of 0.01,
174 0.05, and 0.10 vol.% in concentration using some surfactants. The thermophysical properties
175 of these nanofluids and their base fluids are also evaluated at 20°C. In addition, heat transfer
176 experiments are reported and discussed, showing the impact of surfactants, nanoparticle
177 content, and nature on the heat transfer coefficient and Nusselt number which are compared
178 to theoretical correlations.

179

180 **2. Experimental Methods**

181 **2.1. Nanoparticles and Nanofluid Preparation**

182

183 In this work, commercial copper nanoparticles (Cu) with an average size of 40 nm were
184 purchased from VWR (Alfa Aesar, ROTI®nanoMETIC), while magnetite nanoparticles
185 (Fe_3O_4), nanoporous graphene (NPG), multi-walled carbon nanotubes (MWCNT) were
186 synthesized by our group in the framework of this investigation as described below, prior to
187 specify the method for producing nanofluids. Materials and chemicals used for the synthesis
188 and production of the different nanoparticles and nanofluids were purchased from
189 commercial sources (Sigma–Aldrich and Merck). In all experiments dedicated to the
190 nanoparticles synthesis, deionized water was used.

191 With regards to Fe_3O_4 , the process was yet fully described in [25][28] and used in the similar
192 way. The reader is referred to these works for a full explanation of the synthesis process.

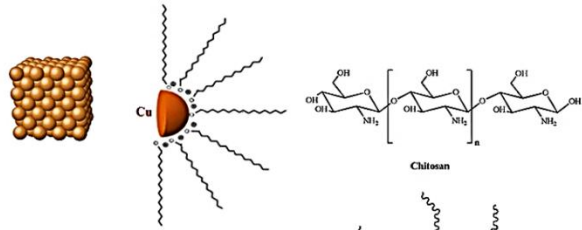
193 Nanoporous graphene was synthesized by chemical vapor deposition (CVD) including
194 methane as the carbon source and hydrogen as the carrier gas in a ratio of 4:1, within a quartz
195 tube (diameter 5 cm, length 120 cm) into an electrical horizontal furnace at temperatures of
196 900-1100°C for 30-45 min. After the growth and cooling process, the product was stirred in
197 18% HCl solution for about 16 h at ambient temperature to obtain pure nanoporous graphene
198 and remove the metal nanocatalysts [29]. Then, the sample was washed repeatedly with
199 deionized water until the neutral product was obtained. Finally, the product was dried in an
200 oven at 100 °C for 12 h.

201 The MWCNTs were produced by CVD consisting of 20% methane in hydrogen over Co–
202 Mo/MgO catalysts [30]. The catalysts were reduced first with the mixture of hydrogen and
203 nitrogen under a flow rate of 200 ml/min. The methane (20% in hydrogen) was used into the
204 reactor as a feed of the reaction. The quartz reactor size is 140 cm in height and 2 cm in inner
205 diameter. A porous quartz disc distributor was used to hold the nanocatalysts. For producing
206 MWCNTs, the reaction temperature was increased from 850°C to 1050°C. The growth of
207 carbon nanotubes was obtained using methane in hydrogen with a flow of 250 ml/min. The
208 synthesized nanoparticles and HCl (18%) mixture were stirred at ambient temperature for 16
209 hours to purify the nanoparticles. Once produced, the MWCNTs were washed with distilled
210 water and dried at 120°C for 8 h.

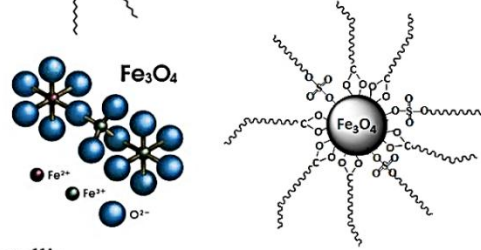
211 For the dispersion and the stabilization of nanoparticles within distilled water considered as
212 the base fluid, different commercial stabilizers and surfactants have been used. Their nature
213 and content are summarized in Figure 1 with the associated nanoparticles.

214

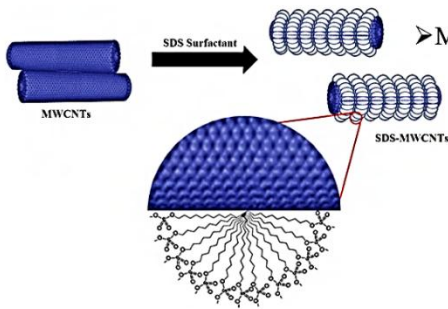
- Copper (Cu) as Metallic nanoparticle
Copper, nano ROTI®nanoMETIC 40nm
0.2 wt% Chitosan (CH) as Stabilizer
0.1 wt% L-ascorbic Acid as a reducing agent



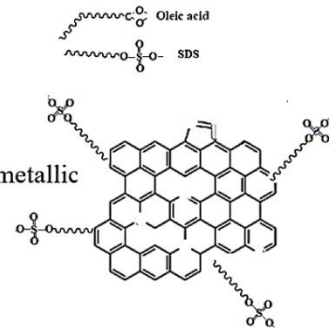
- Fe₃O₄ as Metal oxides
Ultrasonic Co-Precipitation method
0.2 vol% Oleic Acid (OA) and
0.2 wt% Sodium Dodecyl Sulfonate (SDS)



- MWCNT as Non-metallic
CVD method
0.08 wt% SDS as Stabilizer



- Nano porous Graphene as Non-metallic
CVD method
0.1 wt% SDS and
0.1 wt% PVP as Stabilizer



215

216

Figure 1. Overview of nanomaterials and stabilizers used for producing nanofluids

217

Nanofluids were produced adding the required mass of nanoparticles into the base fluid with the corresponding surfactants, see figure 1, using ultrasonic mixing for 15 min. A probe sonicator (Qsonica, USA, LLC 60Hz, Q700W, Sonication Pulse Rate: 1s ON, 1s OFF) was used and the temperature sample was controlled from a cooling jacket during nanofluid preparation. A series of nanofluids with different volume concentrations of nanoparticles were accordingly prepared, 0.01, 0.05, & 0.1% respectively, for each type of nanoparticles, e.g. Cu, Fe₃O₄, MWCNT, and NPG. Such concentrations were obtained from the densities values of nanoparticles reported later in Table 1.

225

2.2. Characterization of Nanomaterials

226

227

As in our previous work [25], X-ray diffraction (XRD) patterns of nanopowders were obtained with X' Pert Pro diffractometer (Philips, PW 1800 X-ray, Netherlands) with Cu Ka (λ = 1.5406 Å) radiation in the angular domain of 10<2θ<80° to identify the crystal structure of nanoparticles. SEM (Philips, XL-30ESEM, Netherlands) was used for direct examination of nanomaterial morphological structure. The size and morphological characterization of the nanoparticles were investigated at a 15 kV operating voltage. The surface area of the molecular sieve and the porosity of nanopowders were evaluated at 77 K using physisorption

233

234 of nitrogen with ELSORP-mini II (BEL Japan Inc., Japan). The associated Data Analysis
235 Software based on the adsorption isotherms was used for determining the BET surface areas
236 of the nanoparticles.

237 **2.3. Thermo-physical properties measurements**

238

239 The thermophysical properties of nanofluids were experimentally evaluated at 20°C. The
240 density of nanofluids was evaluated from the pycnometer method according to ASTM D153.
241 The measurement uncertainty, evaluated with distilled water, is reported to be less than ±
242 0.2%.

243 Dynamic light scattering (DLS) measurement using a Zetasizer Nano S (Malvern
244 Instruments, UK) was performed to evaluate the size of the nanoparticles at 20°C. The
245 samples were prepared using few drops of each nanofluid dispersed in the excess base fluid
246 to achieve an acceptable degree of dilution (approximately 40 times, detection by instrument
247 showing optimum level) for optical clarity, followed by sonication. As previously reported in
248 the literature [17], DLS-size results obtained for low-concentrated dispersions can be
249 representative of dispersion state at slightly higher concentrations.

250 Rheological measurements of the nanofluids were performed with a stress-controlled
251 rheometer (Malvern Instruments Ltd, Malvern Kinexus Pro, UK) with a 60 mm diameter
252 cone-plate configuration, a 1° cone angle, and a 0.03 mm in gap and controlled temperature
253 by a Peltier system implemented into the lower plate. Experiments were conducted at 20°C
254 for base fluids and nanofluids. Rheological flow curves were obtained imposing shear
255 stresses for covering the shear rate range from 10 to 1000 s⁻¹ with at least 10 points per
256 decade. Shear rate and dynamic viscosities were collected under steady-state conditions.
257 Additional details about rheological experiments can be found in Cabaleiro et al. [31]. The
258 viscosity values of water, which behaves in a Newtonian manner as expected for all
259 temperatures, were favorably compared to ASHRAE data [32] with an Absolute Average
260 Deviation (AAD) less than 3%. Experiments were done in 3 replicates for each sample.

261 A THW-L2 Portable thermal conductivity meter (Thermtest Inc., Canada) was used to
262 measure base fluid and nanofluid thermal conductivity at 20°C. This device is based on a
263 quick hot-wire technique according to the ASTM D7896 standard. In the temperature range
264 5/20°C, an AAD less than 1.5% was obtained with distilled water compared to ASHRAE
265 data [32, 33]. Experiments were done according to [28] and the reader can refer to this work

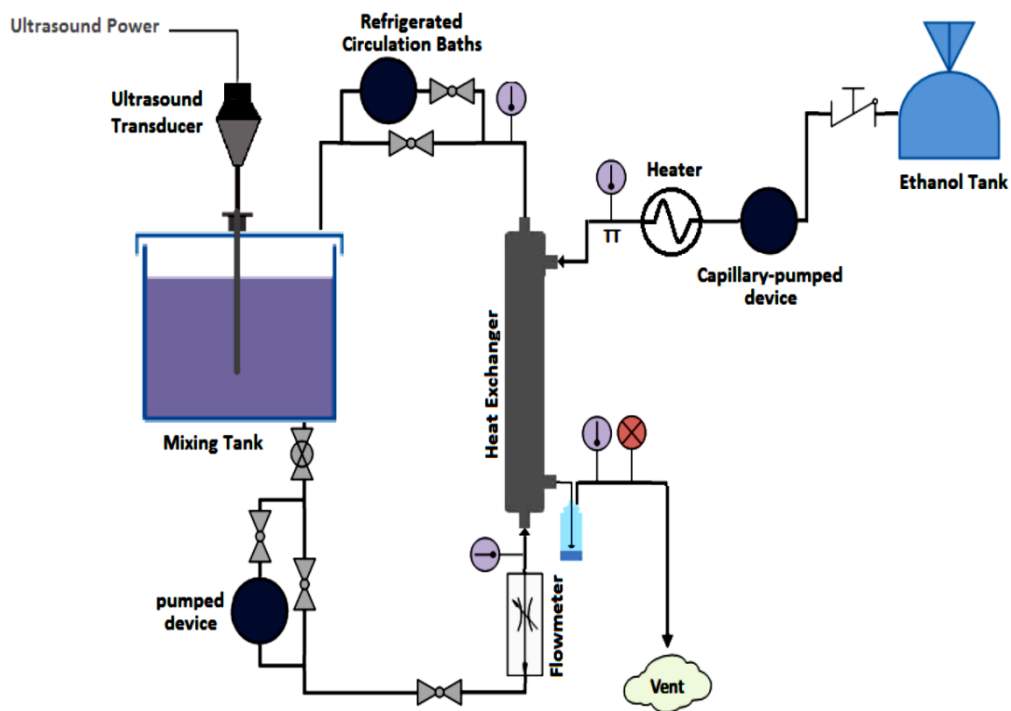
266 for more details. Briefly, a power input varying between 90-110 mW was applied, and a short
267 time of 1.5s was used for thermal conductivity measurement avoiding convection. The
268 experiments were repeated 5 times for each sample, the reported values being an average of
269 these data. Each sample was stayed at the required temperature for at least 1 h before being
270 tested.

271 Finally, the heat capacity of nanoparticles was measured at 20°C by an adiabatic calorimetry
272 device (AK-9.02-BCT-21 calorimeter, TERMAX, Russia) with an uncertainty of 0.2%. The
273 results are the average of three repeated tests.

274 2.4. Heat transfer experiments

275

276 As mentioned in the introduction, the process of evaporation and condensation involves the
277 transfer of heat to and from the product stream, and then the change of the alcohol phase from
278 the liquid to the vapor and vice versa. This phase change requires a lot of added/removal heat
279 at a constant temperature [1]. Such a process can be efficiently realized with heat exchangers.
280 Consequently, the present research reports an experimental study and set-up about the heat
281 transfer evaluation during the ethanol condensation process, as described in Figure 2, and
282 discussed in detail further.



283

284 **Figure 2: Diagram for the HTC experimental set-up for heat transfer experiments.**

285 Ethanol is used to test the condensation process in the heat transfer experiments. At first, the
 286 ethanol is evaporated in the heater and later it is condensed in the heat exchanger. Water-
 287 based nanofluids are considered as heat transfer fluids. A double-shell heat exchanger is used
 288 and was covered with several distinct layers of sponge rubber insulation foam with a high
 289 thermal resistance value (thermal resistance 1.25 K.W^{-1}). K-type thermocouples are
 290 positioned along with the flow for the inlet and outlet of the test section for measuring the
 291 bulk temperatures of nanofluids as well as wall temperature. To ensure a constant temperature
 292 at the inlet of the test section, the heated fluids return to the collection tank passing through a
 293 cooling unit, which is a shell and tube heat exchanger. The temperatures during experimental
 294 runs are recorded with a data acquisition system. Seven different flow rates of fluid into the
 295 cold side were tested in the range $6\text{-}36 \text{ g.s}^{-1}$ varying pump level of the circulator bath. The
 296 flow rate on the hot side (ethanol condensation) is 0.2 g.s^{-1} . The temperature in the cold side
 297 started at 20°C for water-based nanofluids and reaches a maximum of 26°C for the lowest
 298 flow rate of 6 g.s^{-1} because of the ethanol condensing process on the other side of the heat
 299 exchanger. All the data were recorded in the steady-state condition. To ensure consistency,
 300 the tests were replicated twice, and the results were repeated with equal precision. A
 301 manometer was used to measure the liquid pressure drop in the tubing. The pressure drop
 302 uncertainty was evaluated around 0.1% . As it is explained later, different type of water-based
 303 nanofluids were considered, varying also their concentration in nanoparticles, as well as the
 304 flow rate in the heat exchanger to evaluate their performance from heat transfer coefficient
 305 evaluation.

306 2.5. Data Analysis

307 During the experiments, the tube wall temperature, the inlet and outlet temperature of the
 308 sample nanofluid, the mass flow rate as well as the static pressure difference were measured.
 309 Due to the passage of nanofluids through a circular tube, the convective heat transfer
 310 coefficient h and the Nusselt number can be evaluated under laminar flow condition as
 311 follows [34]:

$$312 \bar{h}_{\text{nf}}(\text{exp}) = \frac{Q(\text{exp})}{\pi D_h L (T_w - T_b)_{\text{LM}}} \quad (1)$$

$$313 Q(\text{exp}) = \dot{m}_{\text{nf}} C_{\text{Pnf}} (T_{b1} - T_{b2}) \quad (2)$$

$$314 T_w = T_{\text{win}} - \frac{Q(\text{exp})}{2\pi L_{\text{in}} k_{\text{glass}}} \ln \left(\frac{D_{\text{out}}}{D_{\text{in}}} \right) \quad (3)$$

$$315 \overline{\text{Nu}}_{\text{nf}}(\text{exp}) = \frac{\bar{h}_{\text{nf}}(\text{exp}) D_h}{k_{\text{nf}}} \quad (4)$$

316 Where $(T_w - T_b)_{LM}$ is the average logarithmic temperature difference. D_{in} (45 mm) and D_{out} (65
 317 mm) are inner and outer diameters of the inner tube which has a thermal conductivity of 0.8
 318 $W \cdot m^{-1} \cdot K^{-1}$ (K_{glass}) and L_{in} (1.35 m) is its length. The length of the heat exchanger is $L=0.295$
 319 m and its hydrodynamic diameter is $D_h=31.6$ mm leading to a L/D ratio of around 9.5. T_{win}
 320 and T_w are inner and outer temperature of the wall in the heat exchanger respectively.

321 In order to evaluate the relevance of the experiments and validate the set-up, first, the
 322 measurements were performed using pure water as heat transfer fluid for which correlations
 323 under laminar forced convection in a pipe are well-known. Also, the Nusselt number
 324 predicted by the Seider-Tate equation was compared with the calculated Nusselt equation
 325 using experimental data. The Nusselt number was computed from the following correlation
 326 [35].

$$327 \quad \overline{Nu}_{nf}(th) = 1.86(Re_{nf} Pr_{nf} \frac{D_h}{L})^{1/3} \left(\frac{\mu_{nf}}{\mu_{wnf}} \right)^{0.14} \quad (5)$$

$$328 \quad \overline{h}_{nf}(th) = \frac{\overline{Nu}_{nf}(th) k_{nf}}{D_h} \quad (6)$$

329 This correlation is valid for $100 < Re < 2100$, $0.6 < Pr < 100$, and $L/D < 0.1 Re Pr$.

330 μ_{wnf} is the viscosity of nanofluids at wall temperature. In addition, the following
 331 dimensionless numbers are used for determining the heat transfer coefficient under the
 332 laminar flow of nanofluids through the circular tube.

$$333 \quad Re_{nf} = \frac{\rho_{nf} U D_h}{\mu_{nf}} \quad (7)$$

$$334 \quad Pr_{nf} = \frac{C_{p_{nf}} \mu_{nf}}{k_{nf}} \quad (8)$$

$$335 \quad Pe_{nf} = \frac{U D_h}{\alpha_{nf}} \quad (9)$$

$$336 \quad \alpha_{nf} = \frac{k_{nf}}{\rho_{nf} C_{p_{nf}}} \quad (10)$$

337

338 The thermophysical properties of nanofluids in the previous equations were experimentally
 339 determined as described in section 2.3. With regards to specific heat capacity C_p evaluation,
 340 the following widely used correlation has been considered, at the average bulk temperature of
 341 nanoparticles and water, e.g 20°C [34].

$$342 \quad C_{p_{nf}} = \frac{\phi \rho_{np} C_{p_{np}} + (1-\phi) \rho_{bf} C_{p_{bf}}}{\rho_{nf}} \quad (11)$$

343 All these thermophysical properties will be used in the following to compare theoretical and
 344 experimental heat transfer properties in heat exchanger involved in the ethanol condensation
 345 process described previously. The data in Table 1 provides the needed properties of
 346 nanoparticles and surfactants for all calculations.

347

348 **Table 1: Properties of nanoparticles and surfactants at 20°C.**

Materials/Properties	Density Kg.m ⁻³	Thermal Conductivity W.m ⁻¹ -K ⁻¹	Heat Capacity kJ.kg ⁻¹ .K ⁻¹
Water	998.2 *	0.596 *	4.186 [32]
Cu	8920 **	401 [36]	0.463 *
Fe ₃ O ₄	5180 [28]	17.7 [37]	0.679 *
MWCNT	2100 [14]	3000 [38]	0.857 *
NPG	2200 [39]	5000 [39]	1.211 *
Chitosan	725 **	0.12 [40]	1.04 [40]
Oleic Acid	895 **	0.17 [41]	2.05 [41]
SDS	1010 [42]	0.212 [42]	0.706 [42]
PVP	1200 **	0.105 [43]	1.54 [43]

349 * Experimental value

350 ** Given by producer

351

352 2.6. Uncertainty evaluation

353 The uncertainty of the variables and the calculated parameters were obtained using the
 354 following equation [44]:

$$355 \frac{\Delta R}{R} = \frac{1}{R} \sqrt{\sum_{n=1}^N \left(\frac{\partial R}{\partial x_i} \Delta x_i \right)^2} \quad (12)$$

356 The uncertainty of equipment and devices is reported in Table 2. The uncertainty of the heat
 357 transfer coefficient, Re number, Nu number for water-based nanofluids were evaluated to
 358 ±3.00%, ±3.61%, and ±3.35%, respectively.

359 **Table 2: Accuracy of the measuring instruments.**

Description	Model	Accuracy / Relative accuracy
Temperature	Type K, Thermocouple	± 0. 01°C
Thermal Conductivity	THW-L2, Thermtest Inc.	± 1.5%

Dynamic Viscosity	Rheometer, Malvern Kinexus Pro	$\pm 3\%$
Fluid flow rate	Circulator Bath	$\pm 2\%$
Length (L, D _h)	Vernier Caliper	± 0.02 mm
Density	Pycnometer	$\pm 0.2\%$
Pressure	manometer	$\pm 0.1\%$
Weight	Measuring balance	± 0.0001 g

360

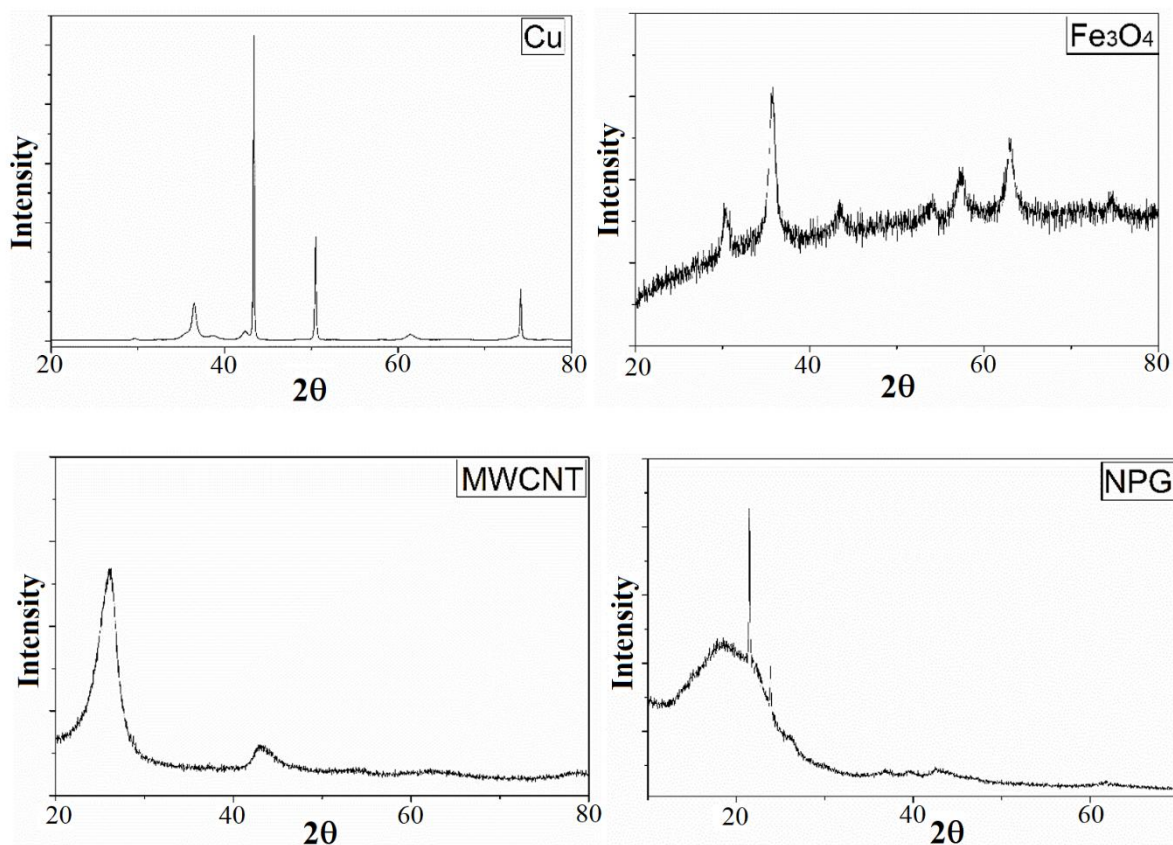
361 **3. Results and Discussion**

362 **3.1. Characterizations of nanoparticles**

363 XRD characterization of nanoparticles used for nanofluids production are reported in Figure
364 3. The average nanoparticles' crystallite sizes were calculated with the Scherrer formula [45].
365 The diffraction peaks for Cu appears at $2\theta = 43.3^\circ$, 50.5° and 74.1° and correspond to
366 crystallographic planes of (111), (200), and (220), respectively (indexed to face-centred cubic
367 crystals with JCPDS card No. 4-836) [46, 47]. Crystallite sizes of Cu nanoparticles possess
368 an average size of 30 nm. Diffraction peaks of the Fe₃O₄ (JCPDS file No. 75-0449) take place
369 at 30.3° , 35.7° , 43.3° , 53.7° , 57.3° , and 62.9° , in agreement with crystallographic planes
370 (220), (311), (400), (422), (511), and (440), respectively, with no indication of the possible
371 presence of α -Fe₂O₃ [12]. The average calculated size for Fe₃O₄ crystal is 10 nm. For NPG
372 XRD patterns, the peaks at $2\theta = 29^\circ$ (corresponding to a d-spacing of 0.30 nm), and 48° , can
373 be observed corresponding to the diffraction of the crystal planes of graphene which could be
374 indexed to the (002) and (100) planes, respectively (JCPDS No. 01-0646) [29, 48]. With
375 MWCNTs, crystallographic (002) and (100) planes are indexed to the main diffraction peaks
376 for MWCNT at $2\theta = 26^\circ$, and 43.5° , respectively [49].

377

378



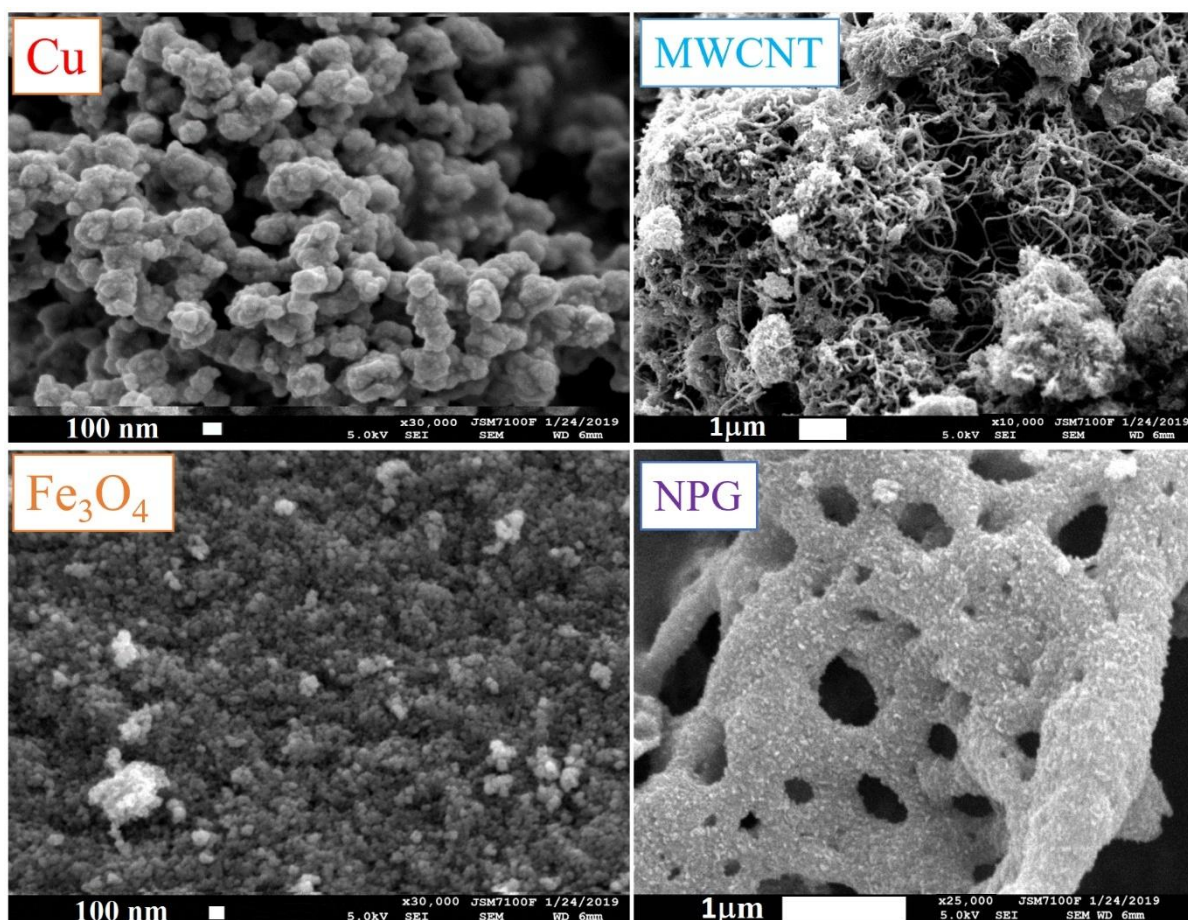
379

380

Figure 3: XRD of nanoparticles.

381 The morphologies of nanoparticles, evaluated from SEM characterization are shown in
 382 Figure 3. Fe₃O₄ nanoparticles appear in form of aggregated spheres with a size from 20 to 60
 383 nm. SEM picture of Cu shows that nanoparticles are almost in a spherical shape and are
 384 rather in aggregated form with the average size in the range 80-160nm. The SEM image also
 385 illustrates the highly porous morphology of the graphene sheets with pore sizes ranging from
 386 0.1 to 1 μm. For MWCNT, a tubular, filamentary, and multi-walled structure of nanotubes
 387 via highly porous network morphology is observed.

388



389

390

Figure 4. FESEM images of nanoparticles.

391 The BET surface area, pore volume (BJH), and the average pore size of Fe₃O₄, Cu, MWCNT,
 392 and NPG are gathered in Table 3.

393 **Table 3: Surface area, pores' size and volume and sizes of the nanoparticles.**

Sample	surface area m ² .g ⁻¹	pore size A°	pore volume cm ³ .g ⁻¹	Average Size (nm)
Fe ₃ O ₄	114	221	0.77	10.1
Cu	15	n.c.	n.c.	45
MWCNT	994	88	1.41	n.c.
NPG	850	99.5	2.11	n.c.

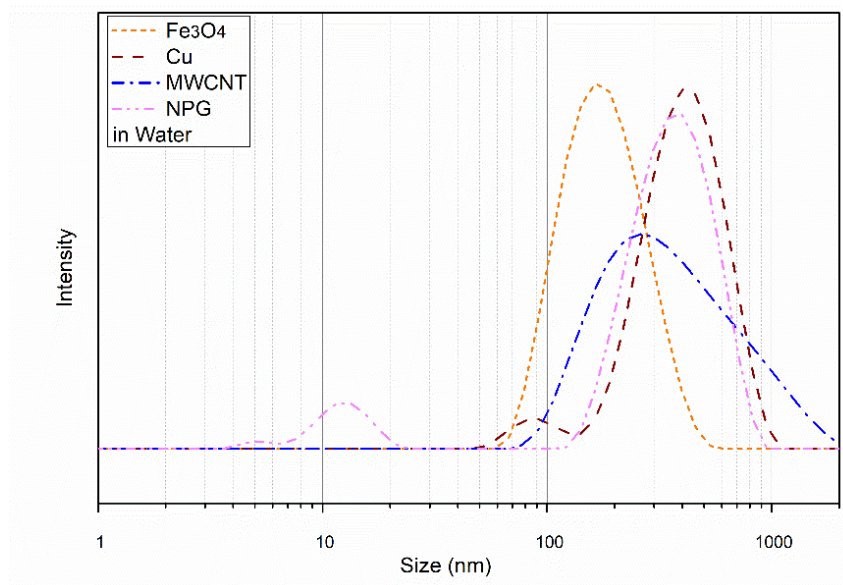
394 n.c.: not calculable

395 The average nanoparticle size d_{BET} approximate as spherical is calculated from the following
 396 equation $d_{BET} = 6000/(\rho \times S_{BET})$. Here, S_{BET} is the surface area (m²/g) and ρ is the skeletal
 397 density (g/cm³) [45]. As shown in Table 3, an average size of 10.1 and 56 nm was evaluated

398 for Fe₃O₄ and Cu nanoparticles respectively, which agrees with crystallite sizes previously
399 reported.

400 The particle size distribution (PSD) of nanoparticles measured by Dynamic Light Scattering
401 (DLS) at 20°C is shown in Figure 5. The average hydrodynamic diameters of Cu, Fe₃O₄,
402 MWCNT, and NPG nanoparticles in water are 373, 164, 296, and 353 nm respectively. PSDs
403 are in agreement with the length and size distribution reported from SEM analysis, but also
404 suggest that nanoparticles can be in the form of small aggregates within water. Figure 5 also
405 shows the presence of double peaks that represent some of the overall fine particles of NPG
406 nanoparticles. It should be pointed out that dynamic light scattering (DLS) measurements are
407 based on the assumption that particles are spherical while the studied NPG nanoadditive are
408 sheet-like shaped and their orientation can play a role. Two-peak and three-peak DLS size
409 distributions were previously found in the literature for other non-spherical nanoparticles [50-
410 52]. In addition, in order to evaluate dispersion ageing throughout time, samples were placed
411 in vials and left at rest under ambient conditions. As evidenced by the Figure 6, the visual
412 inspection of the samples did not show any noticeable sedimentation within several days.

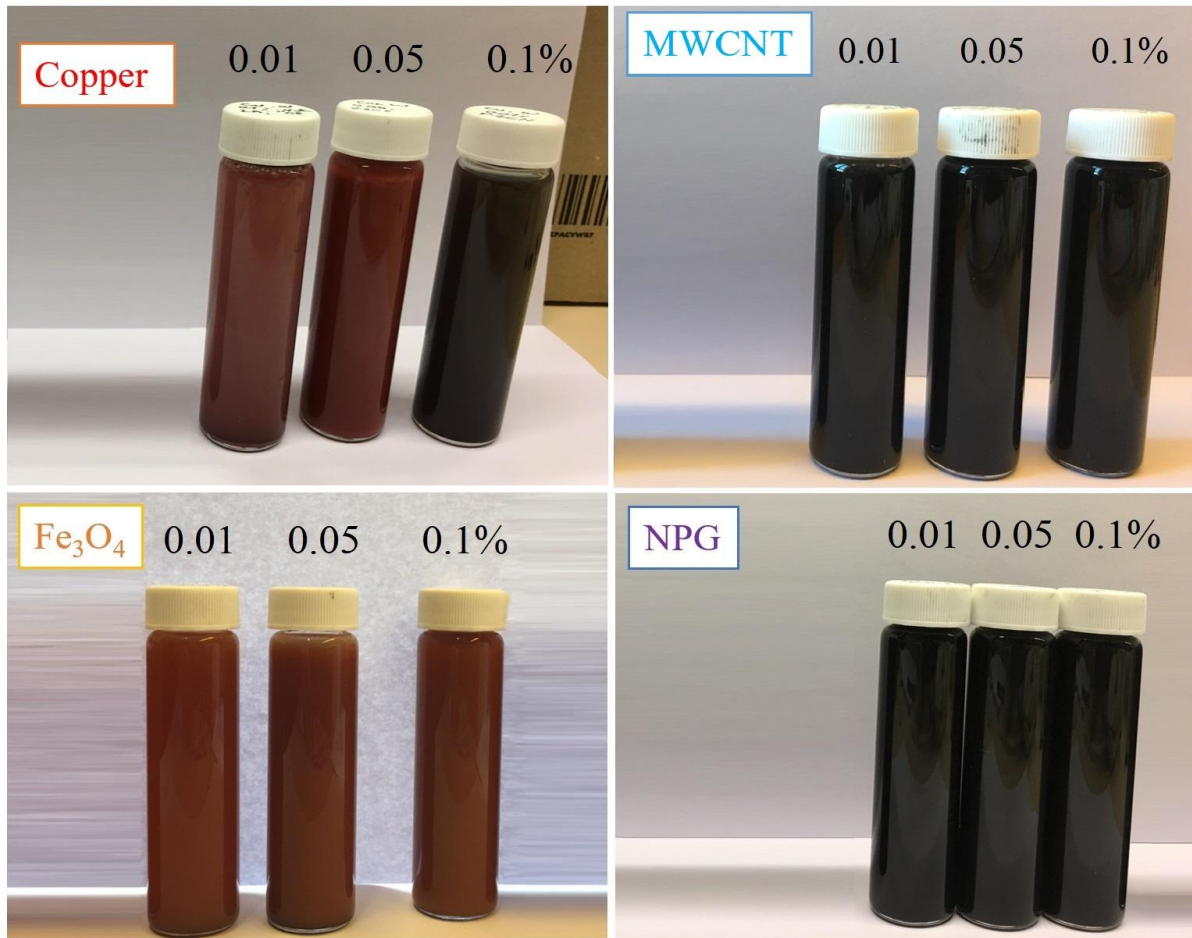
413



414

415

Figure 5. Dynamic light scattering analysis data of diluted nanofluids.



416

417 **Figure 6. Visual aspect of nanofluid sample after 7 days at rest and ambient condition.**

418 **3.2. Thermophysical properties of nanofluids**

419

420 The density values at 20°C of nanofluids are reported in Figure 7. This Figure shows that the
 421 density of nanofluids slightly increases with nanoparticle content. Such a trend is expected
 422 because of the higher density of nanoparticles compared to the base fluid. Placing
 423 nanoparticles between layers of base fluid leads to a slight volume change. This also reduces
 424 the apparent fluid volume, leading to increased volume density per fluid volume [14, 15, 53,
 425 54]. The amount and size of nanoparticles have been shown to influence the total density of
 426 water nanofluid using molecular dynamics [55]. For the higher nanoparticle content, 0.1%,
 427 the increase in density of nanofluids compare to distilled water reaches, 0.8%, 0.4%, 0.4%,
 428 and 0.35% with Cu, Fe₃O₄, NPG, and MWNT respectively. For comparison purposes, the
 429 density experimental data are compared to the classical mixing rule for density, defined by
 430 equation (12) [56].

431
$$\rho_{nf} = \phi \rho_{np} + (1 - \phi) \rho_{bf} \quad (13)$$

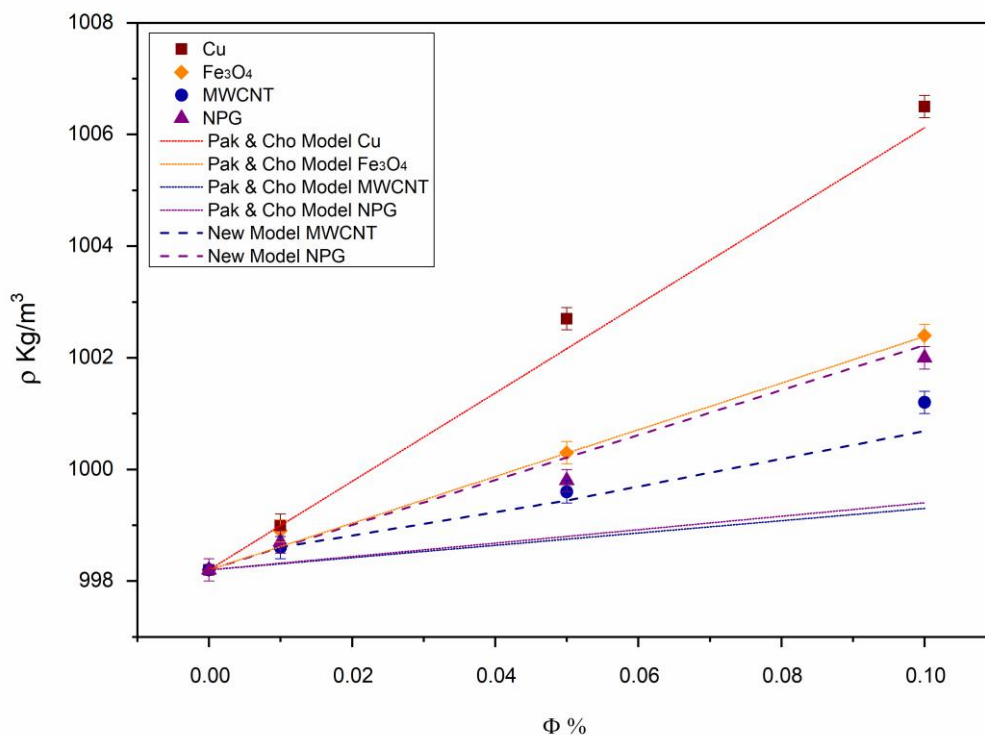
432 Thus, Figure 7 shows that a good agreement is achieved with Cu and Fe₃O₄ nanofluids
 433 between experimental and theoretical data. However, the density of NPG and MWCNT
 434 deviates from equation (12). Such a gap comes from the fact that part of the base fluid can be
 435 adsorbed and trapped within the NPG and MWCNT nanoparticle porosity [53]. The apparent
 436 volume of the fluid can be reduced, and consequently, the density of nanofluid is increased.
 437 Based on this, a theoretical model considering the porosity of nanoparticles is proposed. The
 438 total volume of pore (V_p) obtained from BET characterization (see Table 3) is considered to
 439 refine the density correlation for MWCNT and NPG nanofluids as follows:

$$440 \quad \theta = V_p \rho_{np} \quad (13)$$

$$441 \quad \rho_{nf} = \left(\frac{1}{1+\theta} \right) \phi \rho_{np} + (1 - \phi (1 - \theta)) \rho_{bf} \quad (14)$$

442 A comparison of this theoretical equation and experimental data is also shown in Figure 6. In
 443 that case, a good agreement is achieved, showing the influence of nanoparticle porosity on
 444 the density of carbon nanofluids.

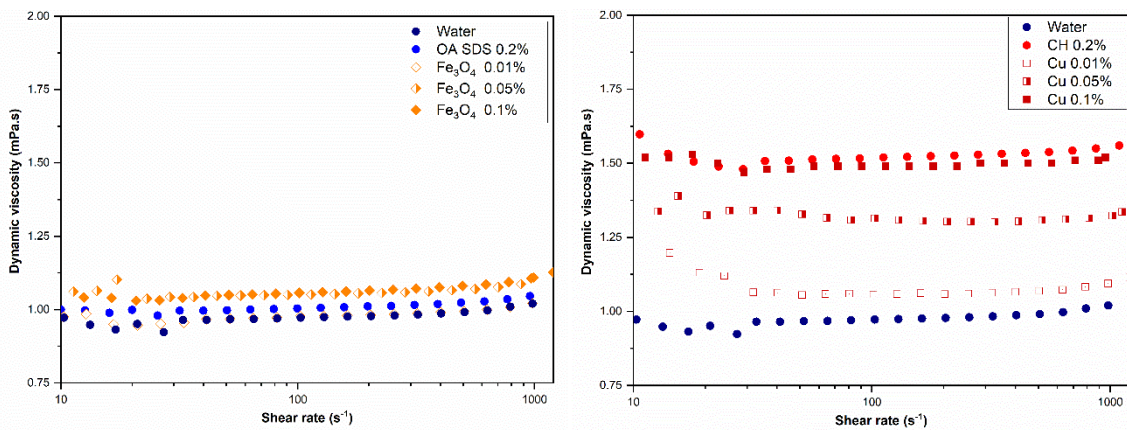
445



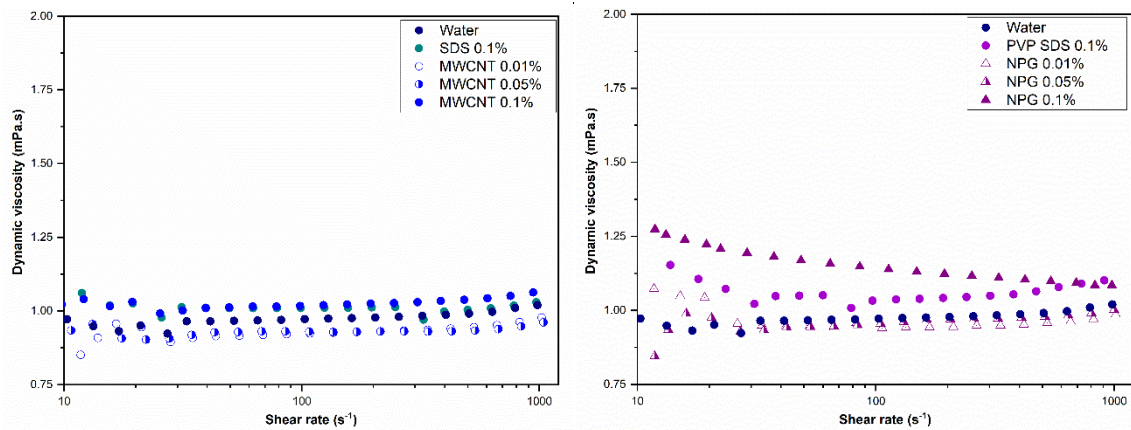
446

447 **Figure 7. Comparison of experimental data of nanofluid density with theoretical**
 448 **models**

449 Figure 8 shows the dynamic viscosity against shear rate for all tested fluids at 20°C. The
 450 figure evidences the difference in rheological behaviour and dynamic viscosity enhancement
 451 following the base fluid used and the type of nanoparticles and their content. With Fe₃O₄,
 452 both base fluid and nanofluids behave in a Newtonian manner, with no significant change of
 453 dynamic viscosity with shear rate (within the experimental uncertainty). The presence of
 454 surfactant slightly increases the viscosity of water. Viscosity of nanofluids is increased with
 455 nanoparticle content with no significant difference for the higher concentrations. For Cu
 456 nanofluids, the trend is different. While the fluids are mainly Newtonian, the viscosity is
 457 increased by 50% with the surfactant. When nanoparticles are added to the base fluid, the
 458 viscosity is decreased with the content until to reach the viscosity of base fluid with the
 459 higher content in nanoparticles. With regards to MWCNT, base fluid and nanofluids are also
 460 Newtonian. For low concentrations, dynamic viscosity appears to be lower than the one of
 461 base fluid, while it is higher for the higher concentration. Finally, NPG nanofluids present
 462 more complex behaviour with slight shear-thinning for the more concentrated nanofluids and
 463 the base fluid. The dynamic viscosity of nanofluids is lower than the one of base fluid for the
 464 two lower concentrations. It is higher by 0.1%. Interestingly, some of the nanofluids have
 465 reduced viscosity showing a lubricating effect of the nanoparticles coupled to respective
 466 surfactant. Some studies [28, 57, 58] also reported that some nanofluids have this lubricating
 467 effect, resulting in a decrease in viscosity.



468



469

470

Figure 8. Dynamic viscosity versus shear rate of water, base fluid and nanofluids at 20°C – Impact of nanoparticle type and content

471

472

473

474

475

476

477

478

479

480

481

482

483

484

485

486

487

488

489

490

491

492

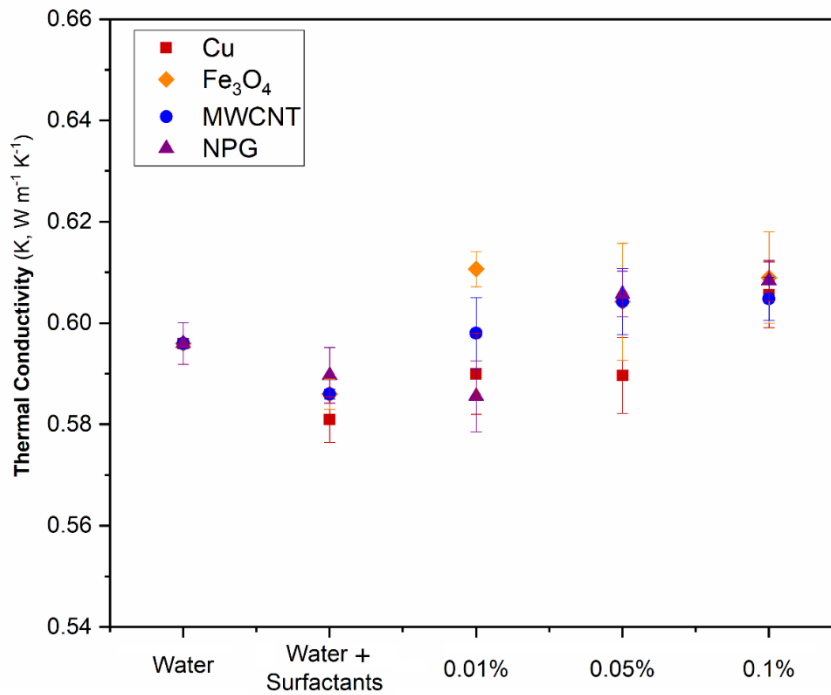
493

494

Figure 9. presents the thermal conductivity of base fluids and water-based nanofluids for different concentrations at 20°C. As a general trend, it is observed that the presence of surfactant/stabilizers, that are used to disperse and stabilize nanoparticles into water, tends to slightly decrease the thermal conductivity of water. This behaviour was also previously reported with different other surfactants [59]. However, a recent study using molecular dynamics simulations evaluated the effect of surfactant volume ratio on the thermal performance of the base fluid, as well as the effect of base liquid and surfactant interactions on the thermal efficiency of the nanofluid. As a result, the surfactant-containing nanofluid's thermal conductivity was greater than the primary nanofluid's [60]. Also, it is shown that the thermal conductivity of nanofluids is increased with nanoparticle content, as generally expected. At the highest value of nanoparticle concentration, the increases in thermal conductivity reach 2%, 3%, 2%, and 5% for Cu, Fe₃O₄, MWCNT, NPG nanofluids, respectively. While nanoparticles have different thermal conductivity values (see Table 1) following their nature, it appears that the thermal conductivity of nanofluids does not vary a lot with the concentrations considered. With the same type of nanoparticles, previous studies have shown an increase in thermal conductivity of water-based nanofluids, typically for Cu, an enhancement of 11% at 0.1 vol.% [61], and 15% at 0.5 wt.% [62] was reported. With Fe₃O₄, previous works showed 7% in thermal conductivity enhancement at 0.1 vol.% [63], and 3% at 0.1 vol.% [64]. For MWCNT, a thermal conductivity increase about 4% at 0.25 vol.% [65], and 6% at 1 vol.% [66] was demonstrated. With graphene, the thermal conductivity increased by 1.4% at 0.1 wt.% [67] and 3.5% at 0.07 wt.% [68]. However, one can noticed that the enhancement we reported here are in the same order of magnitude, while the concentrations considered are low.

495

496

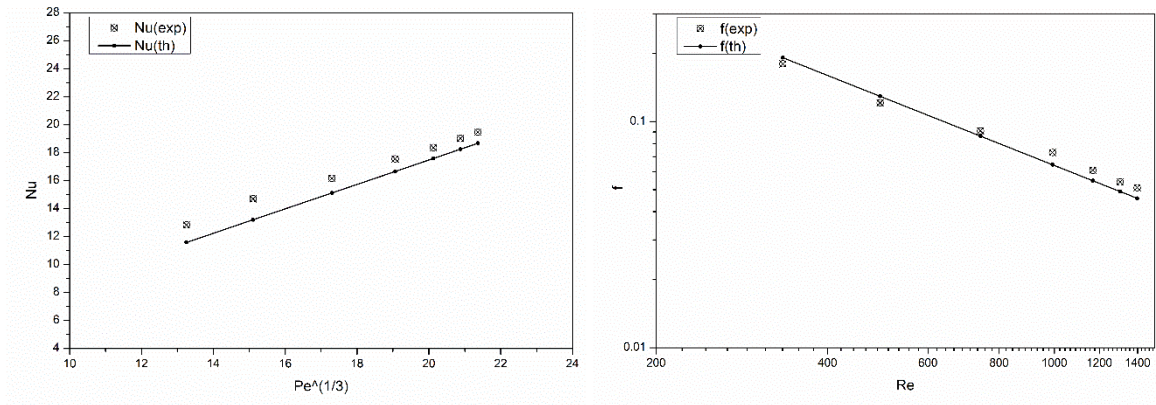


497

498 **Figure 9. Thermal conductivity values of base fluids and nanofluids as a function of**
499 **concentration and type of nanoparticles at 20°C.**

500 **3.3. Heat transfer properties of nanofluids**

501 First, as a validation of the experimental set-up and theoretical analysis, we report in Figure
502 10 the results for distilled water. This Figure gives the evolution of Nu against Pe and friction
503 factor against Re, comparing theoretical and experimental data. The results of the Nu
504 numbers obtained from equation (4) and the experimental values shown in Figure 10 follow
505 the same trend and they are close, with a standard deviation of $\pm 11\%$. Finally, a quite good
506 agreement is achieved between the current study and the relevant predictions defined
507 previously. Moreover, the Figure also demonstrates the good agreement between the wall
508 friction factor f calculated by the Darcy–Weisbach equation $f = 2D\Delta P/\rho u^2 L$ for Newtonian
509 liquids [69] and the classical correlation, $f = 64/Re$ for liquids. Presently, the Reynolds
510 number resulting from pumping power ranges from 300 to 1500.



511

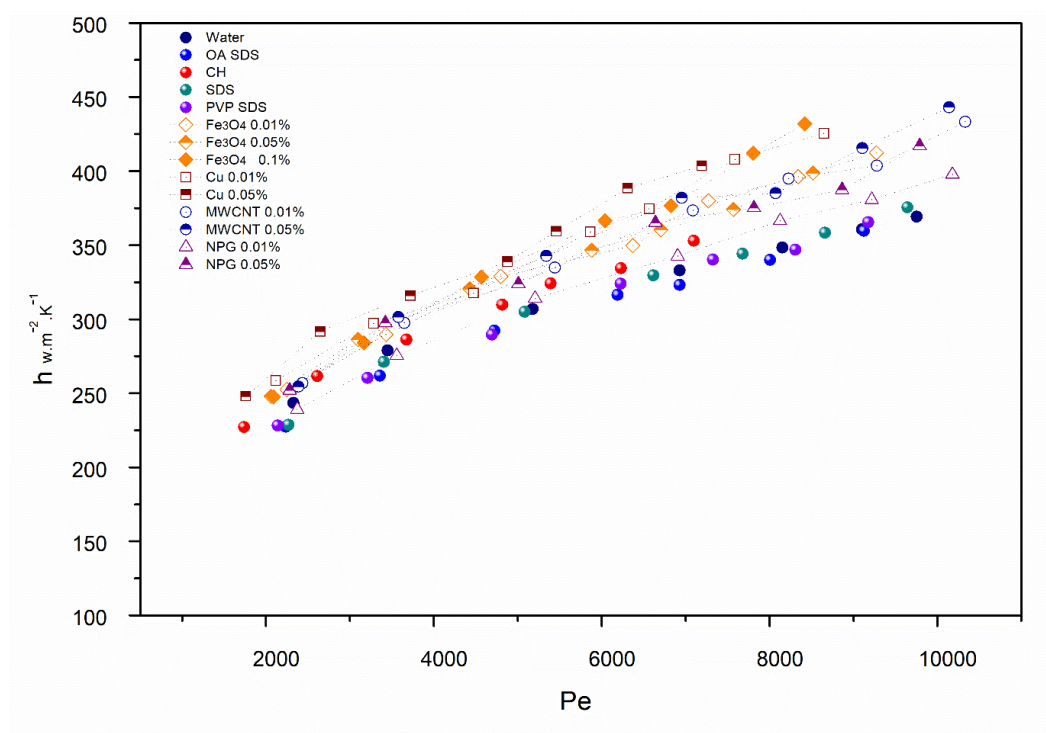
512

Figure 10. Validation of experimental setup at 20°C.

513

514 The convective transfer coefficient h with respect to the Peclet number Pe for water, base
 515 fluids, and nanofluids at 20°C is reported in Figure 11. This Figure shows that the heat
 516 transfer coefficient is increased with Pe and some differences can be noticed between base
 517 fluids and nanofluids, as well as with the nature of nanoparticle and their content.

518

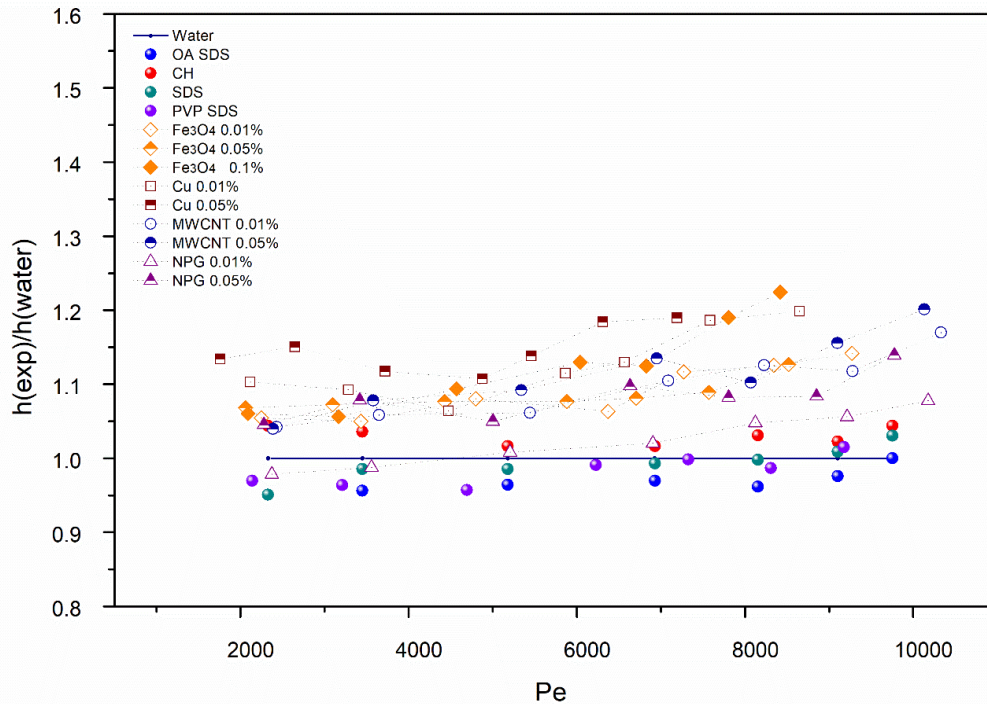


519

520 **Figure 11. Base fluids and nanofluids heat transfer coefficient as a function of Peclet**
 521 **number.**

522

523 To get a clear picture of the different impacts of surfactant and nanoparticle nature and
524 content on heat transfer coefficient compared to pure distilled water, Figure 12 shows the
525 heat transfer coefficient ratio of both base fluids and nanofluids to water.



526

527 **Figure 12. Ratio of base fluids and nanofluids' heat transfer coefficient to water heat**
528 **transfer coefficient vs Peclet number**

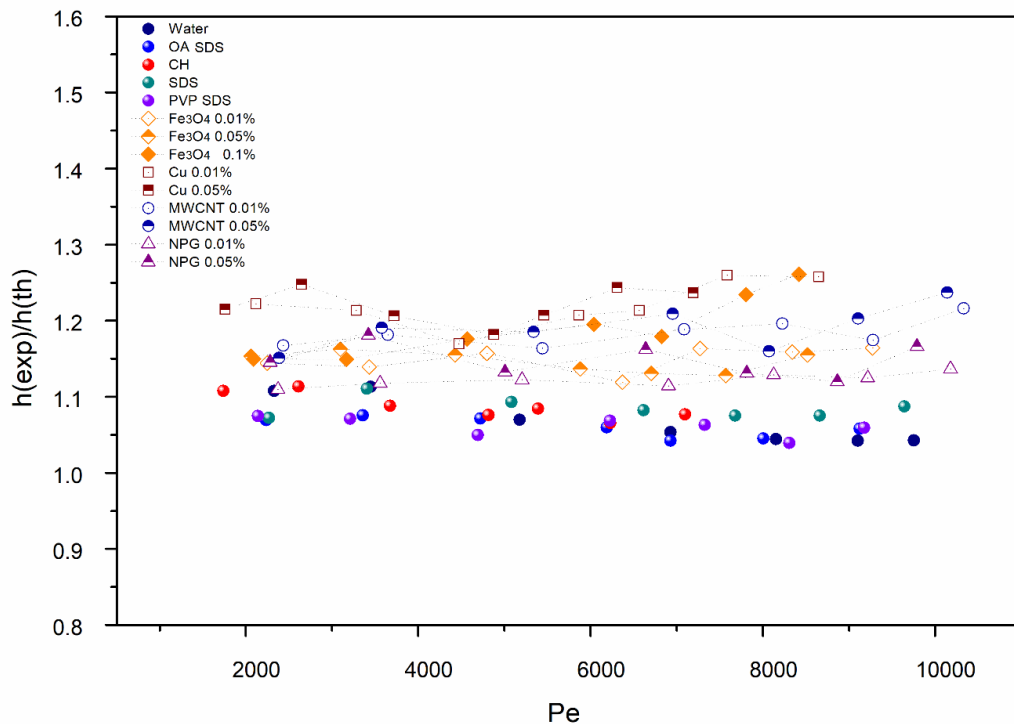
529 First, it is observed that surfactants alone do not induce similar results. The presence of some
530 surfactants can penalize the heat transfer coefficient of water, as the ratio is lower than 1.
531 That is mainly the case for the mixture of PVP SDS and OA SDS. With SDS alone, in the
532 range of Pe number, the ratio is lower than 1 for low Pe number, while it is higher than 1 for
533 high Pe number. For CH, the ratio is always higher than one. Then, nanoparticles addition to
534 base fluids improves the heat transfer coefficient as the ratio is higher than 1, and can reach
535 up to 20% in enhancement. Hence, all nanofluids have a higher coefficient of heat transfer
536 than distilled water while the thermal conductivity of nanofluids was not greatly improved
537 with nanoparticles. The results show that the higher the percentage of nanoparticles in the
538 fluid, the higher is the heat transfer ratio. From previous findings, it is known that the heat
539 transfer coefficient increases with an increase in the concentration of nanoparticles [3, 70].
540 Actually, Cu, Fe₃O₄, MWCNT, and NPG nanofluids have higher heat transfer coefficients

541 than water. The enhancements compared to water are 13, 7, 4, and 4.5% for Cu, Fe₃O₄,
542 MWCNT, and NPG nanofluids at 0.05 vol.% respectively, at a low Peclet number of 2300.
543 This enhancement reaches 18, 12, 10, and 8.5% at high Peclet number (8000), respectively
544 for Cu, Fe₃O₄, MWCNT, and NPG nanofluids at 0.05 vol.%. Such an enhancement can be
545 attributed to the coupled effect, at these low concentrations, of the slight thermal conductivity
546 increase while the viscosity is moderately increased or even decreased compared to water.
547 Finally, among all nanofluids and concentrations, Cu nanofluids provide the best
548 enhancement in heat transfer compare to water in the entire range of Pe number. High
549 enhancement is also obtained for Fe₃O₄ and MWCNT but only at higher Pe numbers. These
550 results are consistent with previous studies. Actually, although the heat transfer geometry,
551 nanomaterials, and experimental conditions are not fully identical, our results can be
552 compared with some studies. For example, it has been reported that the local heat transfer
553 coefficient at Re = 1600 has increased by 8% for Al₂O₃ water-based nanofluids at 0.6 vol. %,
554 the thermal conductivity of this nanofluid being around 3.5 % higher than the base fluid [9].
555 Other works with water-based nanofluids reported a heat transfer enhancement of 5% for
556 Al₂O₃ nanofluids (0.2 vol.%) and 6% with CuO nanofluids (0.2 vol.%) at Peclet number of
557 5000 [10]. Also, changing the Pe number from 2500 to 6000 leads to an heat transfer increase
558 from 8 to 16% for Al₂O₃ nanofluids (0.2 vol.%) [12]. Similarly, a heat transfer enhancement
559 about 6 % was obtained with MWNTs nanofluid (0.1 wt.%) and NPG nanofluid (0.1 wt.%)
560 at 33 °C [15]. Such an enhancement reaches 11.8 % for CNT nanofluids (0.055 wt.%) in [16]
561 and 5.4, 10.3 and 19.1% with Al₂O₃ nanofluids with the following concentrations 0.03, 0.14
562 and 0.3 vol.%, respectively [18]. In addition, an increase in Re number from 200 to 1000
563 rises the heat transfer coefficient from 6 to 20% for Al₂O₃ nanofluids (4 vol.%) and 8 to 16%
564 for TiO₂ nanofluids (4 vol.%) respectively [20]. Finally, it is observed that the heat transfer
565 enhancement presently reported can reach higher value while the concentration in
566 nanoparticles is lower.

567

568 Furthermore, Figure 13 presents the convective heat transfer coefficient ratio of both base
569 fluids and nanofluids to the theoretical value defined previously in section 2.5. The
570 nanofluid's heat transfer coefficients are significantly higher than theoretical values, as seen
571 in Figure 13. Particle size, materials, shape and concentration, type of base fluids, surfactant,
572 boundary condition, and range of Reynolds number are critical considerations for evaluating

573 their effect on the heat transfer coefficient in the laminar flow in circular tubes [71, 72].
 574 Although nanofluid heat transfer behavior depends on the volume fraction, average size and
 575 species of nanoparticles, and flow conditions [73, 74]. The reported difference in heat transfer
 576 coefficient is correlated to different factors and mechanisms not included in the theoretical
 577 development. A better prediction for nanofluids heat transfers could be found by analysing
 578 factors such as the interaction flow structure and the collision intensity of nanoparticles, as
 579 well as the dispersion and relative movement of these particles throughout the vicinity of the
 580 tube wall, the temperature profile, and the thickness of the boundary layer [18, 75]. For
 581 example, the temperature near the wall tends to be greater than that used for calculation, and
 582 the properties of nanofluids can evolve during heat transfer, as the temperature slightly
 583 increases during the condensation process, thereby enhancing the nanofluid's heat transfer.
 584 The strong effect of particle properties on fluid and the impact of nanofluid composition on
 585 flow and heat transfer properties, experimental uncertainty, a key mechanism of nanofluid
 586 flow, can be the source of the gap between experimental data and theoretical prediction.



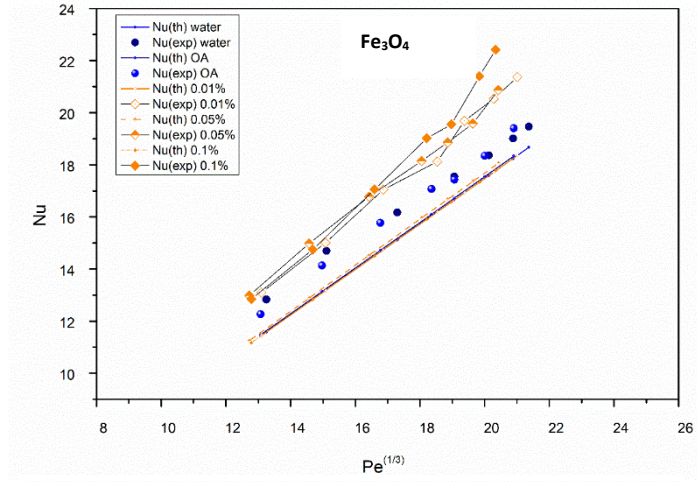
587
 588 **Figure 13. Ratio of base fluids and nanofluids' heat transfer coefficient**
 589 **to theoretical heat transfer coefficient in function of Peclet number**

590 Nusselt numbers are shown in Figure 14 with respect to the Peclet number for all base fluids
 591 and water-based nanofluid at various concentrations. Experimental values are also compared

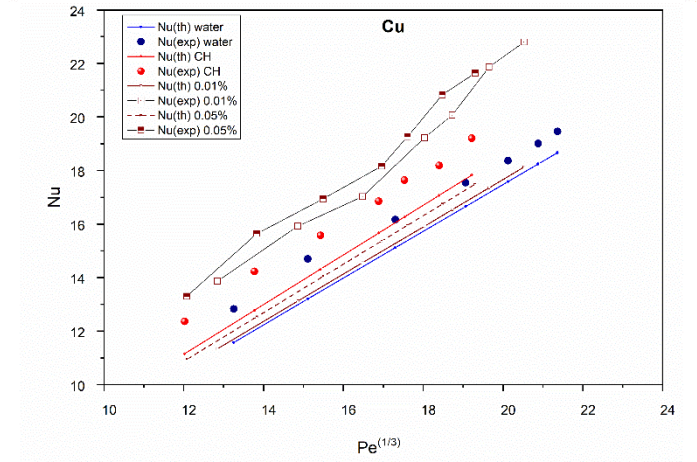
592 to theoretical ones. Thus, the Nusselt number increases with an increase in the Peclet for all
593 fluids. The increase is greater for nanofluids, compared to base fluids, with an increase in the
594 percentage of nanoparticles, particularly in higher Peclet. Additionally, previous research
595 indicates that increasing the Reynolds number (which results in an increase in the number of
596 Peclet) and the volume concentration of particles increases the Nusselt number [12, 20]. For
597 example, Nusselt numbers increased by approximately 9.9, 20.9, and 29.8% for Al_2O_3
598 nanofluids at the highest tested Reynolds number for volume concentration of 0.03, 0.14, and
599 0.3, respectively [18]. The Nusselt number of all fluids, however, is greater than the
600 theoretical number calculated by Seider-Tate's correlation (Equation 5), but the increasing
601 trend is consistent with the theoretical calculation. Although it was reported in [20] that the
602 number of Nusselt depends to a small extent on the type of nanoparticles, other work [10]
603 shows that the increase in Nusselt number for Al_2O_3 water nanofluid is greater than the
604 increase in Nusselt number for CuO water nanofluid. Nevertheless, the results of this study
605 show that, in addition to the type of nanomaterials used, type of surfactants can
606 fundamentally change Nusselt numbers by altering thermophysical properties of nanofluids.

607

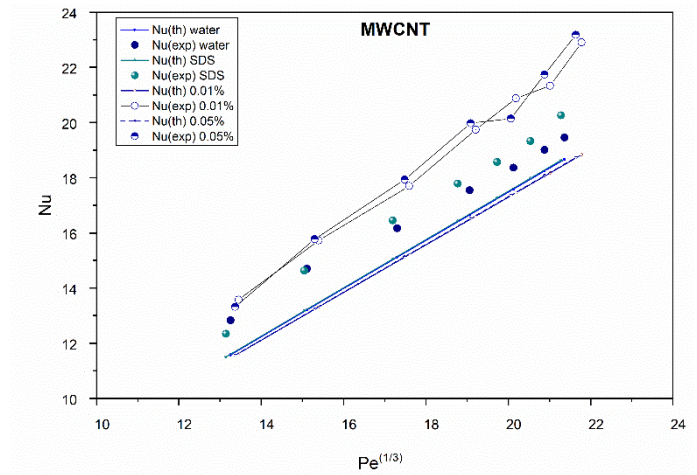
608

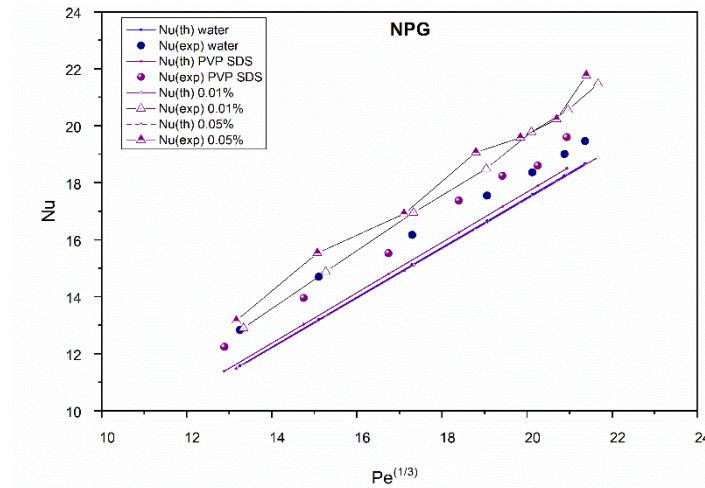


609



610





611

612

Figure 14. Nusselt number of base fluids and water-based nanofluids versus Peclet number at 20°C. – Influence of nanoparticle nature and concentration

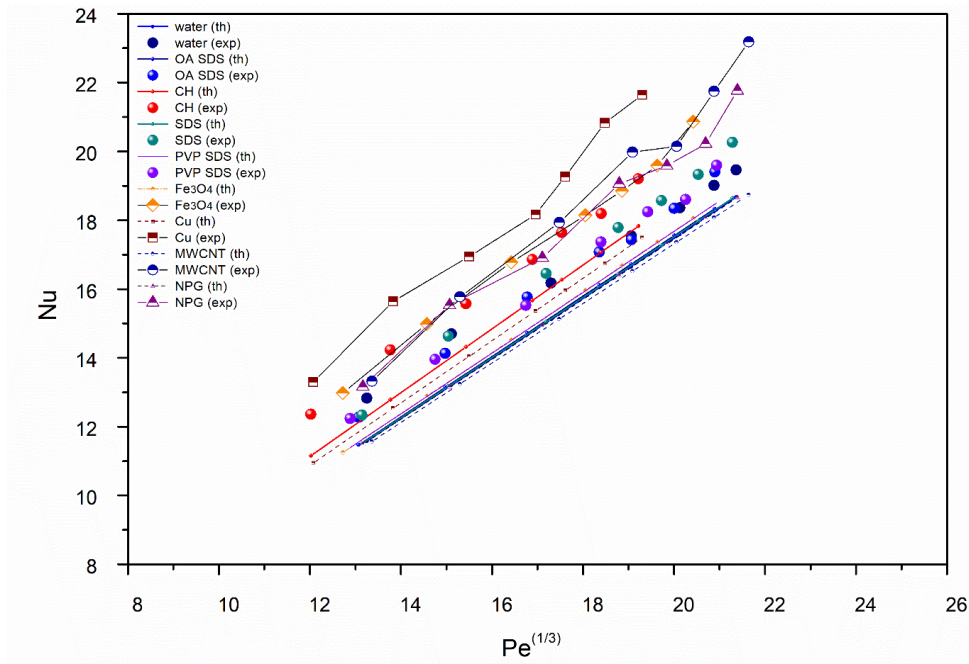
613

614

For comparison purposes between nanofluids, the Nusselt number with respect to the Peclet number for all water-based nanofluids with 0.05% in vol. at 20°C are gathered in Figure 15. The pattern of Nusselt number with Peclet number for all nanofluids is consistent with the data obtained from theoretical calculations, as also shown previously in Figure 13. At low $Pe=2300$, the Nusselt numbers are enhanced by 12%, 4.5%, 2.5%, and 2.5% for Cu, Fe₃O₄, MWCNT, and NPG nanofluids, respectively, at 0.05 vol%. At high $Pe=8000$, the Nusselt numbers are enhanced by 22%, 12%, 10%, and 8% for Cu, Fe₃O₄, MWCNT, and NPG nanofluids, respectively at the same concentration. Consequently, as evidenced by heat transfer coefficient evolution, the best nanofluid is based on copper nanoparticles.

623

624



625

626 **Figure 15. Nu number of base fluids and water-based nanofluids at 0.05 vol.% in**
 627 **respect Peclet number at 20°C.**

628 **4. Conclusion**

629

630 We reported in this paper the heat transfer properties of water-based nanofluids during the
 631 ethanol condensation process. Different types of nanoparticles were considered for nanofluids
 632 preparation, including Cu, Fe₃O₄, MWCNT, and NPG in volume fraction from 0.01 to 0.1%.
 633 Different surfactants have been used to produce nanofluids. The comprehensive
 634 characterization of the nanoparticles has been completed including XRD, SEM, BET surface
 635 area, and DLS analysis. Then, the density, thermal conductivity, and rheological properties of
 636 nanofluids were experimentally evaluated. It was shown that the density of nanofluids
 637 increases with nanoparticle content, this trend is correlated to nanoparticle porosity with
 638 carbon-based nanoparticles. The thermal conductivity of nanofluid was reported to slightly
 639 increase with nanoparticle volume fraction. The nanofluids mainly behave as Newtonian
 640 fluids in the shear rate range investigated. Following the type of nanoparticles, the viscosity
 641 can increase or decrease with nanoparticle concentration, showing a lubricating effect of
 642 nanoparticles coupled with respective surfactants.

643 In addition, it was demonstrated that the heat transfer properties, heat transfer coefficient, and
 644 Nusselt number, are increased with nanofluids compared to water and base-fluids, up to 20%.
 645 The results are slightly dependant on the type of nanoparticles and concentration. The

646 addition of nanoparticles can significantly enhance heat transfer performance at low and high
647 Peclet numbers for tested water-based nanofluids. Also, it was shown that these experimental
648 heat transfer properties are higher than those predicted by theoretical correlations, while
649 experimental thermophysical were used. Finally, based on our results, copper nanofluids
650 appear to be the best candidate for the application and pipe flow geometry considered.

651

652 **Acknowledgements**

653 A.B. acknowledges the Research Institute of Petroleum Industry (RIPI) as well as EU COST
654 for the STSM grant ref. COST-STSM-CA15119-42469 linked to the Cost Action
655 “Overcoming Barriers to Nanofluids Market Uptake (NANOUP TAKE)”. A.B. also
656 acknowledges the Centre for Thermogravimetric and Calorimetric Research of Research park
657 of St. Petersburg State University. P.E. acknowledges the European Union through the
658 European Regional Development Fund (ERDF), the Ministry of Higher Education and
659 Research, the French region of Brittany and Rennes Métropole for the financial support of
660 thermal conductivity experimental device.

661

662

663

664 **References**

- 665 [1] W.L. Mc Cabe, J.C. Smith, P. Harriott, Unit operation of chemical engineering, McGraw-
666 Hill 2018.
- 667 [2] P. Krajnik, A. Rashid, F. Pušavec, M. Remškar, A. Yui, N. Nikkam, M.S. Toprak,
668 Transitioning to sustainable production – part III: Developments and possibilities for
669 integration of nanotechnology into material processing technologies, *Journal of Cleaner*
670 *Production*, 112 (2016) 1156–1164.
- 671 [3] D. Wen, G. Lin, S. Vafaei, K. Zhang, Review of nanofluids for heat transfer applications,
672 *Particuology*, 7 (2009) 141–150.
- 673 [4] R.S. Vajjha, D.K. Das, A review and analysis on influence of temperature and
674 concentration of nanofluids on thermophysical properties, heat transfer and pumping power,
675 *International Journal of Heat and Mass Transfer*, 55 (2012) 4063–4078.
- 676 [5] S.A. Angayarkanni, J. Philip, Review on thermal properties of nanofluids: Recent
677 developments, *Advances in colloid and interface science*, 225 (2015) 146–176.
- 678 [6] M. Patil, S. Kim, J.-H. Seo, M.-Y. Lee, Review of the Thermo-Physical Properties and
679 Performance Characteristics of a Refrigeration System Using Refrigerant-Based Nanofluids,
680 *Energies*, 9 (2016) 22.

681 [7] S. Javed, H.M. Ali, H. Babar, M.S. Khan, M.M. Janjua, M.A. Bashir, Internal convective
682 heat transfer of nanofluids in different flow regimes: A comprehensive review, *Physica A:*
683 *Statistical Mechanics and its Applications*, 538 (2020) 122783.

684 [8] J. Pérez-Tavernier, J. Vallejo, D. Cabaleiro, J. Fernández-Seara, L. Lugo, Heat transfer
685 performance of a nano-enhanced propylene glycol: Water mixture, *International Journal of*
686 *Thermal Sciences*, 139 (2019) 413-423.

687 [9] D. Wen, Y. Ding, Experimental investigation into convective heat transfer of nanofluids
688 at the entrance region under laminar flow conditions, *International journal of heat and mass*
689 *transfer*, 47 (2004) 5181-5188.

690 [10] S.Z. Heris, S.G. Etemad, M.N. Esfahany, Experimental investigation of oxide nanofluids
691 laminar flow convective heat transfer, *International communications in heat and mass*
692 *transfer*, 33 (2006) 529-535.

693 [11] Y. He, Y. Jin, H. Chen, Y. Ding, D. Cang, H. Lu, Heat transfer and flow behaviour of
694 aqueous suspensions of TiO₂ nanoparticles (nanofluids) flowing upward through a vertical
695 pipe, *International journal of heat and mass transfer*, 50 (2007) 2272-2281.

696 [12] S.Z. Heris, M.N. Esfahany, S.G. Etemad, Experimental investigation of convective heat
697 transfer of Al₂O₃/water nanofluid in circular tube, *International journal of heat and fluid flow*,
698 28 (2007) 203-210.

699 [13] P. Garg, J.L. Alvarado, C. Marsh, T.A. Carlson, D.A. Kessler, K. Annamalai, An
700 experimental study on the effect of ultrasonication on viscosity and heat transfer performance
701 of multi-wall carbon nanotube-based aqueous nanofluids, *International Journal of Heat and*
702 *Mass Transfer*, 52 (2009) 5090-5101.

703 [14] R.L. S. Askari, A. Seifkordi, A.M. Rashidi, H. Koolivan, A novel approach for energy
704 and water conservation in wet cooling towers by using MWNTs and nanoporous graphene
705 nanofluids, *Energy Conversion and Management* 109 (2016) 10–18.

706 [15] S. Askari, Lotfi, R., Rashidi, A.M., Koolivand, H., Koolivand-Salooki, M. ,
707 Rheological and thermophysical properties of ultra-stable kerosenebased Fe₃O₄/Graphene
708 nanofluids for energy conservation, *Energy Conversion and Management*, 128 (2016) 134–
709 144.

710 [16] P. Estellé, S. Halefadi, T. Maré, Thermophysical properties and heat transfer
711 performance of carbon nanotubes water-based nanofluids, *Journal of Thermal Analysis and*
712 *Calorimetry*, 127 (2017) 2075-2081.

713 [17] L. Colla, L. Fedele, M. Buschmann, Laminar mixed convection of TiO₂–water nanofluid
714 in horizontal uniformly heated pipe flow, *International Journal of Thermal Sciences*, 97
715 (2015) 26-40.

716 [18] R. Barzegarian, A. Aloueyan, T. Yousefi, Thermal performance augmentation using
717 water based Al₂O₃-gamma nanofluid in a horizontal shell and tube heat exchanger under
718 forced circulation, *International Communications in Heat and Mass Transfer*, 86 (2017) 52-
719 59.

720 [19] Emad Sadeghinezhad, Mohammad Mehrli, R. Saidur, Mehdi Mehrli, Sara Tahan
721 Latibari, Amir Reza Akhiani, H.S.C. Metselaar, A comprehensive review on graphene
722 nanofluids: Recent research, development and applications, *Energy Conversion and*
723 *Management*, 111 (2016) 466–487.

724 [20] D. Guzei, A. Minakov, V.Y. Rudyak, On efficiency of convective heat transfer of
725 nanofluids in laminar flow regime, *International Journal of Heat and Mass Transfer*, 139
726 (2019) 180-192.

727 [21] Z. Wang, F. Han, Y. Ji, W. Li, Performance and exergy transfer analysis of heat
728 exchangers with graphene nanofluids in seawater source marine heat pump system, *Energies*,
729 13 (2020) 1762.

730 [22] Y. Khelili, A. Allali, R. Bouakkaz, Studies on Cu and TiO₂ Water-based Nanofluids: A
731 Comparative Approach in Laminar Flow, (2018).

732 [23] M.S. Kamel, F. Lezsovits, Simulation of nanofluids laminar flow in a vertical channel,
733 Pollack Periodica, 13 (2018) 147-158.

734 [24] M.R. Gholami, O.A. Akbari, A. Marzban, D. Toghraie, G.A.S. Shabani, M.
735 Zarringhalam, The effect of rib shape on the behavior of laminar flow of oil/MWCNT
736 nanofluid in a rectangular microchannel, Journal of Thermal Analysis and Calorimetry, 134
737 (2018) 1611-1628.

738 [25] Q. Gravndyan, O.A. Akbari, D. Toghraie, A. Marzban, R. Mashayekhi, R. Karimi, F.
739 Pourfattah, The effect of aspect ratios of rib on the heat transfer and laminar water/TiO₂
740 nanofluid flow in a two-dimensional rectangular microchannel, Journal of Molecular Liquids,
741 236 (2017) 254-265.

742 [26] S. Babita, S.K., Gupta S. M., Preparation and evaluation of stable nanofluids for heat
743 transfer application: A review, Experimental Thermal and Fluid Science 79 (2016) 202–212.

744 [27] H. Babar, H.M. Ali, Towards hybrid nanofluids: preparation, thermophysical properties,
745 applications, and challenges, Journal of Molecular Liquids, 281 (2019) 598-633.

746 [28] A. Banisharif, M. Aghajani, S. Van Vaerenbergh, P. Estellé, A. Rashidi, Thermophysical
747 properties of water ethylene glycol (WEG) mixture-based Fe₃O₄ nanofluids at low
748 concentration and temperature, Journal of Molecular Liquids, 302 (2020) 112606.

749 [29] A. Naghash, S. Sattari, A. Rashidi, Experimental assessment of convective heat transfer
750 coefficient enhancement of nanofluids prepared from high surface area nanoporous graphene,
751 International Communications in Heat and Mass Transfer, 78 (2016) 127–134.

752 [30] Roghayeh Lotfi, Ali Morad Rashidi, A. Amrollahi, Experimental study on the heat
753 transfer enhancement of MWNT-water nanofluid in a shell and tube heat exchanger,
754 International Communications in Heat and Mass Transfer, 39 (2012) 108–111.

755 [31] D. Cabaleiro, P. Estellé, H. Navas, A. Desforges, B. Vigolo, Dynamic Viscosity and
756 Surface Tension of Stable Graphene Oxide and Reduced Graphene Oxide Aqueous
757 Nanofluids, Journal of Nanofluids, 7 (2018) 1081-1088.

758 [32] A.H. Fundamentals, Physical properties of secondary coolants, Amer. Soc. Heating, Ref.
759 Air-Conditioning Eng. Inc., Atlanta, GA, (2005).

760 [33] S. Hamze, N. Berrada, D. Cabaleiro, A. Desforges, J. Ghanbaja, J. Gleize, D. Bégin, F.
761 Michaux, T. Mare, B. Vigolo, Few-layer graphene-based nanofluids with enhanced thermal
762 conductivity, Nanomaterials, 10 (2020) 1258.

763 [34] M.T.H. Mosavian, S.Z. Heris, S.G. Etemad, M.N. Esfahany, Heat transfer enhancement
764 by application of nano-powder, Journal of Nanoparticle Research, 12 (2010) 2611–2619.

765 [35] S. Zeinali Heris, S.G. Etemad, M. Nasr Esfahany, Experimental investigation of oxide
766 nanofluids laminar flow convective heat transfer, International Communications in Heat and
767 Mass Transfer, 33 (2006) 529–535.

768 [36] M. Liu, M.C. Lin, C. Wang, Enhancements of thermal conductivities with Cu, CuO, and
769 carbon nanotube nanofluids and application of MWNT/water nanofluid on a water chiller
770 system, Nanoscale research letters, 6 (2011) 1-13.

771 [37] K.K. Varma, P. Kishore, P.D. Prasad, Enhancement of heat transfer using Fe₃O₄/water
772 nanofluid with varying cut-radius twisted tape inserts, International Journal of Applied
773 Engineering Research, 12 (2017) 7088-7095.

774 [38] A. Nasiri, M. Shariaty-Niasar, A.M. Rashidi, R. Khodafarin, Effect of CNT structures on
775 thermal conductivity and stability of nanofluid, International Journal of heat and Mass
776 transfer, 55 (2012) 1529-1535.

777 [39] A. Ghozatloo, A. Rashidi, M. Shariaty-Niassar, Convective heat transfer enhancement of
778 graphene nanofluids in shell and tube heat exchanger, Experimental Thermal and Fluid
779 Science, 53 (2014) 136-141.

780 [40] E. Kashtanov, V. Uryash, N.Y. Kokurina, V. Larina, Effect of hydrolysis on heat
781 capacity, thermodynamic functions, and the relaxation transition of crab chitin and chitosan,
782 Russian Journal of Physical Chemistry A, 88 (2014) 221-229.

783 [41] T.V. Oommen, C.C. Claiborne, High oleic acid oil compositions and methods of making
784 and electrical insulation fluids and devices comprising the same, Google Patents, 2006.

785 [42] N.M. van Os, J.R. Haak, L.A.M. Rupert, Physico-chemical properties of selected
786 anionic, cationic and nonionic surfactants, Elsevier 2012.

787 [43] W.S. Khan, N.N. Hamadneh, W.A. Khan, Prediction of thermal conductivity of
788 polyvinylpyrrolidone (PVP) electrospun nanocomposite fibers using artificial neural network
789 and prey-predator algorithm, PloS one, 12 (2017) e0183920.

790 [44] R.J. Moffat, Describing the uncertainties in experimental results, Experimental thermal
791 and fluid science, 1 (1988) 3-17.

792 [45] A. Banisharif, A.A. Khodadadi, Y. Mortazavi, A. Anaraki Firooz, J. Beheshtian, S.
793 Agah, S. Menbari, Highly active Fe₂O₃-doped TiO₂ photocatalyst for degradation of
794 trichloroethylene in air under UV and visible light irradiation: Experimental and
795 computational studies, Applied Catalysis B: Environmental, 165 (2015) 209-221.

796 [46] L. Qing-Ming, T. Yasunami, K. Kuruda, M. Okido, Preparation of Cu nanoparticles with
797 ascorbic acid by aqueous solution reduction method, Trans. Nonferrous Met. Soc. China, 22
798 (2012) 2198–2203.

799 [47] M. Seyedsadjadi, P. Mashayekhshams, he Effect of Polyvinylpyrrolidone on the
800 Formation of Copper Nanoplates in Wet-Chemical Reduction Method, Int. J. Bio-Inorg.
801 Hybd. Nanomat., 1 (2012) 209-214.

802 [48] M.-L. Chen, C.-Y. Park, J.-G. Choi, W.-C. Oh, Synthesis and Characterization of Metal
803 (Pt, Pd and Fe)-graphene Composites, Journal of the Korean Ceramic Society, 48 (2011) 147-
804 151.

805 [49] A. Saravanan, K. Prasad, N. Gokulakrishnan, R. Kalavani, T. Somanathan, Efficiency
806 of Transition Metals in Combustion Catalyst for High Yield Helical Multi-Walled Carbon
807 Nanotubes, Advanced Science, Engineering and Medicine, 6 (2014) 809-813.

808 [50] S. Sen Gupta, V. Manoj Siva, S. Krishnan, T. Sreeprasad, P.K. Singh, T. Pradeep, S.K.
809 Das, Thermal conductivity enhancement of nanofluids containing graphene nanosheets,
810 Journal of Applied Physics, 110 (2011) 084302.

811 [51] P. Dhar, S. Sen Gupta, S. Chakraborty, A. Pattamatta, S.K. Das, The role of percolation
812 and sheet dynamics during heat conduction in poly-dispersed graphene nanofluids, Applied
813 Physics Letters, 102 (2013) 163114.

814 [52] D. Cabaleiro, L. Colla, S. Barison, L. Lugo, L. Fedele, S. Bobbo, Heat transfer capability
815 of (ethylene glycol+ water)-based nanofluids containing graphene nanoplatelets: Design and
816 thermophysical profile, Nanoscale research letters, 12 (2017) 1-11.

817 [53] A.K. Hamid Shirkhanloo, Hassan Zavvar Mousavi, Alimorad Rashidi, , Ultrasound
818 assisted-dispersive-ionic liquid-micro-solid phase extraction based on carboxyl-
819 functionalized nanoporous graphene for speciation and determination of trace inorganic and
820 organic mercury species in water and caprine blood samples, Microchemical Journal January,
821 130 (2017) 245-254.

822 [54] S. Askari, H. Koolivand, M. Pourkhalil, R. Lotfi, A. Rashidi, Investigation of
823 Fe₃O₄/Graphene nanohybrid heat transfer properties: Experimental approach, International
824 Communications in Heat and Mass Transfer 87 (2017) 30–39.

825 [55] R.B. Dehkordi, D. Toghraie, M. Hashemian, F. Aghadavoudi, M. Akbari, Molecular
826 dynamics simulation of ferro-nanofluid flow in a microchannel in the presence of external
827 electric field: Effects of Fe₃O₄ nanoparticles, International Communications in Heat and Mass
828 Transfer, 116 (2020) 104653.

829 [56] B.C. Pak, Y.I. Cho, Hydrodynamic and heat transfer study of dispersed fluids with
830 submicron metallic oxide particles, *Experimental Heat Transfer an International Journal*, 11
831 (1998) 151-170.

832 [57] T.X. Phuoc, M. Massoudi, R.-H. Chen, Viscosity and thermal conductivity of nanofluids
833 containing multi-walled carbon nanotubes stabilized by chitosan, *International Journal of*
834 *Thermal Sciences*, 50 (2011) 12-18.

835 [58] L. Chen, H. Xie, W. Yu, Y. Li, Rheological Behaviors of Nanofluids Containing Multi-
836 Walled Carbon Nanotube, *Journal of Dispersion Science and Technology*, 32 (2011) 550-
837 554.

838 [59] P. Estellé, S. Halelfadl, T. Maré, Lignin as dispersant for water-based carbon nanotubes
839 nanofluids: impact on viscosity and thermal conductivity, *International Communications in*
840 *Heat and Mass Transfer*, 57 (2014) 8-12.

841 [60] N.H. Abu-Hamdeh, R.A. Bantan, A. Golmohammadzadeh, D. Toghraie, The thermal
842 properties of water-copper nanofluid in the presence of surfactant molecules using molecular
843 dynamics simulation, *Journal of Molecular Liquids*, 325 (2021) 115149.

844 [61] R. Kathiravan, R. Kumar, A. Gupta, R. Chandra, Preparation and pool boiling
845 characteristics of copper nanofluids over a flat plate heater, *International Journal of Heat and*
846 *Mass Transfer*, 53 (2010) 1673-1681.

847 [62] M. Kole, T.K. Dey, Thermal performance of screen mesh wick heat pipes using water-
848 based copper nanofluids, *Applied Thermal Engineering*, 50 (2013) 763-770.

849 [63] M. Afrand, D. Toghraie, N. Sina, Experimental study on thermal conductivity of water-
850 based Fe₃O₄ nanofluid: development of a new correlation and modeled by artificial neural
851 network, *International Communications in Heat and Mass Transfer*, 75 (2016) 262-269.

852 [64] T.-H. Tsai, L.-S. Kuo, P.-H. Chen, C.-T. Yang, Thermal conductivity of nanofluid with
853 magnetic nanoparticles, *PIERS online*, 5 (2009) 231-234.

854 [65] Y. Hwang, Y. Ahn, H. Shin, C. Lee, G. Kim, H. Park, J. Lee, Investigation on
855 characteristics of thermal conductivity enhancement of nanofluids, *Current Applied Physics*,
856 6 (2006) 1068-1071.

857 [66] I. Garbadeen, M. Sharifpur, J. Slabber, J. Meyer, Experimental study on natural
858 convection of MWCNT-water nanofluids in a square enclosure, *International*
859 *Communications in Heat and Mass Transfer*, 88 (2017) 1-8.

860 [67] W.S. Sarsam, A. Amiri, S. Kazi, A. Badarudin, Stability and thermophysical properties
861 of non-covalently functionalized graphene nanoplatelets nanofluids, *Energy Conversion and*
862 *Management*, 116 (2016) 101-111.

863 [68] Y. Gao, H. Wang, A.P. Sasmito, A.S. Mujumdar, Measurement and modeling of thermal
864 conductivity of graphene nanoplatelet water and ethylene glycol base nanofluids,
865 *International Journal of Heat and Mass Transfer*, 123 (2018) 97-109.

866 [69] I. Lienhard, H. John, A heat transfer textbook, phlogiston press2005.

867 [70] R. Lotfi, Y. Saboohi, A. Rashidi, Numerical study of forced convective heat transfer of
868 nanofluids: comparison of different approaches, *International Communications in Heat and*
869 *Mass Transfer*, 37 (2010) 74-78.

870 [71] S.Z. Heris, S.G. Etemad, M.N. Esfahany, Convective heat transfer of a Cu/water
871 nanofluid flowing through a circular tube, *Experimental heat transfer*, 22 (2009) 217-227.

872 [72] K.S. Hwang, S.P. Jang, S.U. Choi, Flow and convective heat transfer characteristics of
873 water-based Al₂O₃ nanofluids in fully developed laminar flow regime, *International journal*
874 *of heat and mass transfer*, 52 (2009) 193-199.

875 [73] H. Xie, Y. Li, W. Yu, Intriguingly high convective heat transfer enhancement of
876 nanofluid coolants in laminar flows, *Physics Letters A*, 374 (2010) 2566–2568.

877 [74] J. Sarkar, A critical review on convective heat transfer correlations of nanofluids,
878 *Renewable and sustainable energy reviews*, 15 (2011) 3271-3277.

879 [75] K. Anoop, T. Sundararajan, S.K. Das, Effect of particle size on the convective heat
880 transfer in nanofluid in the developing region, International journal of heat and mass transfer,
881 52 (2009) 2189-2195.

882